Geochemistry, Geophysics, Geosystems®

AGU ADVANCING EARTH AND SPACE SCIENCES

RESEARCH ARTICLE
10.1029/2023GC011210

Magnetization of Ferromanganese Crusts: Geochemical and Magnetic Insights From Rio Grande Rise and Tropic Seamount

Muhammad Bin Hassan[1,2,3], Andrea Koschinsky[2,4], Gabriel Lucas Xavier da Silva[5], Rafaela Cardoso Dantas[1,6], Thomas Kuhn[7], Christian Millo[1], Gunther Kletetschka[8,9], and Luigi Jovane[1]

[1]Instituto Oceanográfico, Universidade de São Paulo, São Paulo, Brazil, [2]Department of Physics and Earth Sciences, Constructor University, Bremen, Germany, [3]itt OCEANEON, Technological Institute for Paleoceanography and Climate Changes, UNISINOS University, São Leopoldo, Brazil, [4]Center for Marine Environmental Sciences (MARUM), University of Bremen, Bremen, Germany, [5]Department of Transdisciplinary Science and Engineering, Tokyo Institute of Technology, Tokyo, Japan, [6]Instituto de Geociências - Universidade de São Paulo, São Paulo, Brazil, [7]Federal Institute for Geosciences and Natural Resources (BGR), Hannover, Germany, [8]Faculty of Science, Institute of Hydrogeology, Engineering Geology and Applied Geophysics, Charles University, Prague, Czech Republic, [9]Geophysical Institute, University of Alaska - Fairbanks, Fairbanks, AK, USA

Abstract Ferromanganese (FeMn) crusts are Fe and Mn oxides that typically form on deep-sea elevations by deposition of colloids from seawater. These mineral deposits are considered a source of critical metals and rare earth elements. Besides their potential economic value, FeMn crusts are extremely relevant in ocean science, since their very slow growth rates result in long-term paleoenvironmental and paleoceanographic records. In this study, we applied geochemical, mineralogical, and magnetic analyses to unravel paleoenvironmental changes at two locations on opposite sides of the Atlantic Ocean, the Rio Grande Rise in the SW Atlantic and the Tropic Seamount in the NE Atlantic. Our results show that the occurrence of amorphous (non-crystalline) Fe oxyhydroxides and the absence of Fe oxides in hydrogenetic, non-phosphatized FeMn crusts prevented the development of primary remanent magnetization. In contrast, phosphatized FeMn crusts may have contained a remanent magnetic signal. Phosphatization resulted from increased primary productivity and occurred at different stages during the growth of the FeMn crusts, leading to suboxic conditions and partial dissolution of pre-existing, remanence-carrying magnetic minerals. Carbonate Fluorapatite (CFA) accumulation in the phosphatized layers of FeMn crusts replaced Fe and Mn, decreasing their magnetic content. Thus, magnetic variations do not reflect a primary magnetization but rather result from geochemical alterations. The loss of primary magnetization may hamper the use of FeMn deposits for magnetostratigraphic purposes.

Key Points:

- The hydrogenetic FeMn crusts from the Atlantic Ocean contain paramagnetic/superparamagnetic Fe oxyhydroxides
- Phosphatization events throughout the formation history of FeMn crusts have altered the primary geochemical and magnetic signals
- Biogenic magnetite in FeMn crusts is influenced by the local environment; further research is needed on other influencing factors

Supporting Information:

Supporting Information may be found in the online version of this article.

Correspondence to:

M. B. Hassan,
muhammadbinhassan@alumni.usp.br;
muhammadbinhassan@usp.br;
muhammadbinhassan6@gmail.com

Citation:

Hassan, M. B., Koschinsky, A., da Silva, G. L. X., Dantas, R. C., Kuhn, T., Millo, C., et al. (2024). Magnetization of ferromanganese crusts: Geochemical and magnetic insights from Rio Grande Rise and Tropic Seamount. *Geochemistry, Geophysics, Geosystems*, *25*, e2023GC011210. https://doi.org/10.1029/2023GC011210

Received 31 AUG 2023
Accepted 15 MAY 2024

Author Contributions:

Conceptualization: Muhammad Bin Hassan, Andrea Koschinsky, Luigi Jovane
Data curation: Muhammad Bin Hassan, Gabriel Lucas Xavier da Silva, Rafaela Cardoso Dantas
Formal analysis: Muhammad Bin Hassan

1. Introduction

Deep-sea ferromanganese (FeMn) deposits represent the most significant, yet least explored, asset of 'E-tech' elements on our planet (Hein et al., 2003, 2010, 2012). These deposits include manganese-copper-nickel enriched nodules and cobalt-platinum, and heavy Rare Earth Elements enriched crusts (Hein et al., 2003). In deep ocean setting, FeMn deposits are mainly composed of Fe-oxyhydroxides and Mn oxides accreting at rates of a few millimeters per million year (mm/My) over tens of millions of years, thereby accumulating significant amounts of trace elements from seawater (e.g., Koschinsky & Hein, 2003).

FeMn crusts typically form on hard-rock substrates, on the flanks and summits of seamounts, ridges, and plateaus where the substrate has been swept clean of sediments for millions of years (Hein et al., 2000). They grow by chemical precipitation from seawater at water depths below the oxygen minimum zone (OMZ) (typically deeper than ~700 m) throughout the ocean basins. The Pacific Ocean contains the largest amount of FeMn crusts because there is the largest number of seamounts. The highest abundance of FeMn crusts is in the central and western equatorial Pacific (from 0° to 20°N), in the area referred to as the Pacific Prime Crust Zone. FeMn crusts are also found in the Atlantic and Indian Oceans and in the polar seas, where their mapping is still largely incomplete (Konstantinova et al., 2017). The typical average thickness of FeMn crust varies from 2 to 4 cm to >12 cm (Usui et al., 2007), with a general correlation between the age of the seamount hosting FeMn crusts and crust thickness (Usui & Someya, 1997).

Methodology: Muhammad Bin Hassan, Gabriel Lucas Xavier da Silva, Rafaela Cardoso Dantas, Thomas Kuhn, Christian Millo, Gunther Kletetschka
Resources: Muhammad Bin Hassan, Thomas Kuhn, Gunther Kletetschka, Luigi Jovane
Supervision: Andrea Koschinsky, Luigi Jovane
Visualization: Rafaela Cardoso Dantas, Thomas Kuhn, Christian Millo, Gunther Kletetschka
Writing – original draft: Muhammad Bin Hassan
Writing – review & editing: Andrea Koschinsky, Gabriel Lucas Xavier da Silva, Rafaela Cardoso Dantas, Thomas Kuhn, Christian Millo, Gunther Kletetschka, Luigi Jovane

Atlantic crusts differ in their chemical composition from Pacific crusts, due to a stronger content of terrestrial components in the Atlantic (Hein et al., 2013; Koschinsky et al., 1995).

Given their extremely low growth rate, FeMn crusts conceal clues about the chemistry of the past ocean and are ideal archives for paleoceanographic research (Josso et al., 2019; Koschinsky & Hein, 2017). Previous studies have shown that the vertical variability of the distribution of trace elements in the FeMn crust provides clues about the temporal variability of ocean circulation patterns, and continental erosion rates (Bau & Koschinsky, 2006; Frank et al., 1999; Yi et al., 2023) and redox state in the global ocean (Hein et al., 2003). Moreover, a variety of elements concentrated in FeMn crusts, such as Co, Ti, Mn, Ni, Pt, Zr, Nb, Te, Bi, W, Th, Ni, Cu, Co, Mn, and Mo, are considered critical for the development of carbon-free energy production (Marino et al., 2018). This aspect is also raising concern about the adverse consequence of future deep-sea mining on marine ecosystems, which makes FeMn deposits particularly interesting to both science and society.

Recently, Josso et al. (2019) and Benites et al. (2020) described the genesis of FeMn crusts at two locations on opposite sides of the Atlantic Ocean, the Tropic Seamount (TS, NE Atlantic) and the Rio Grande Rise (RGR, SW Atlantic). In both locations, FeMn crusts underwent extensive diagenetic changes resulting in the formation of Carbonate Fluorapatite (CFA) under suboxic conditions (Benites et al., 2020; Josso et al., 2019; Marino et al., 2017; Sousa et al., 2021). The oldest layers of FeMn crusts from the RGR underwent phosphatization during the Miocene (Benites et al., 2020), while in the TS crusts phosphatization started 38 My ago (Josso et al., 2019).

Magnetic minerals are iron-bearing minerals that occur in nature as oxides, hydroxides, and sulphides. These minerals are sensitive to oxidative and reductive environmental conditions (Liu et al., 2012; Roberts, 2015). Their precipitation is chemically controlled by the concentration of Fe, pH, and redox potential (Emerson et al., 2012). The process of microbial magnetite mineralization in FeMn crusts is still poorly documented. Magnetic analyses of FeMn crusts and nodules from the Pacific Ocean and the China Sea indicated that the primary source of remanent magnetization can be linked to magnetotactic bacteria (Hassan et al., 2020; Jiang, Sun, et al., 2020; Jiang, Zhao, et al., 2020; Oda et al., 2018; Yuan et al., 2020). Although magnetite biomineralization has been reported for hydrogenetic FeMn deposits, most of the Fe-bearing phase is nanometric, X-ray amorphous Fe hydroxide and poorly crystalline Fe-bearing vernadite (Bogdanova et al., 2008; Guan et al., 2017; Hein & Koschinsky, 2014; Jiang et al., 2021), which can also precipitate abiotically.

Several studies have presented magnetostratigraphic dating of FeMn crusts from the Pacific Ocean and the China Sea based on magnetic scanning techniques, as well as traditional cryogenic magnetic methods (Joshima & Usui, 1998; Noguchi, Oda, et al., 2017, Noguchi, Yamamoto, et al., 2017; Oda et al., 2011, 2023; Usui et al., 2017; Yi et al., 2020, 2023; Yuan et al., 2017), whereas magnetic studies on FeMn crusts from the Atlantic Ocean are scarce. In this study, we compare the magnetic properties and geochemical composition of phosphatized and non-phosphatized hydrogenetic FeMn crusts collected in the RGR and in the TS to document the primary source of magnetization and the effect of phosphatization on the magnetic properties of FeMn crusts.

2. Study Areas

2.1. Rio Grande Rise

The RGR is located approximately 1,300 km east of the Brazilian coastline and is separated by the Vema Channel from São Paulo Plateau (Figure 1). The rise is a shallow plateau with a water depth of 800 m separated by a rift structure which is over 1,400 m deep and 900 km long that splits the plateau into two parts, the Western Rio Grande Rise and the Eastern Rio Grande Rise (Camboa & Rabinowitz, 1984) (Figure 1). The Great Rift is 24 km wide and has deep troughs with vertical sides similar to a canyon. The RGR summit is located above the OMZ, which is ventilated by oxygenated Antarctic Intermediate Water (AAIW) and less oxygenated South Atlantic Mode Water (Ayers & Strutton, 2013; Sarmiento et al., 2004).

The basaltic walls are up to 600 m in height. The RGR is a large igneous province of the Cretaceous age. Its origin is still controversial and debatable (Barker et al., 1983; Camboa & Rabinowitz, 1984). Fe-Mn crusts from RGR exhibit two distinct generations. The older generation, estimated to have initiated around 48–55 Ma, underwent extensive post-depositional processes under suboxic conditions, leading to phosphatization during the Miocene period (from 20 to 6.8 Ma) (Benites et al., 2020).

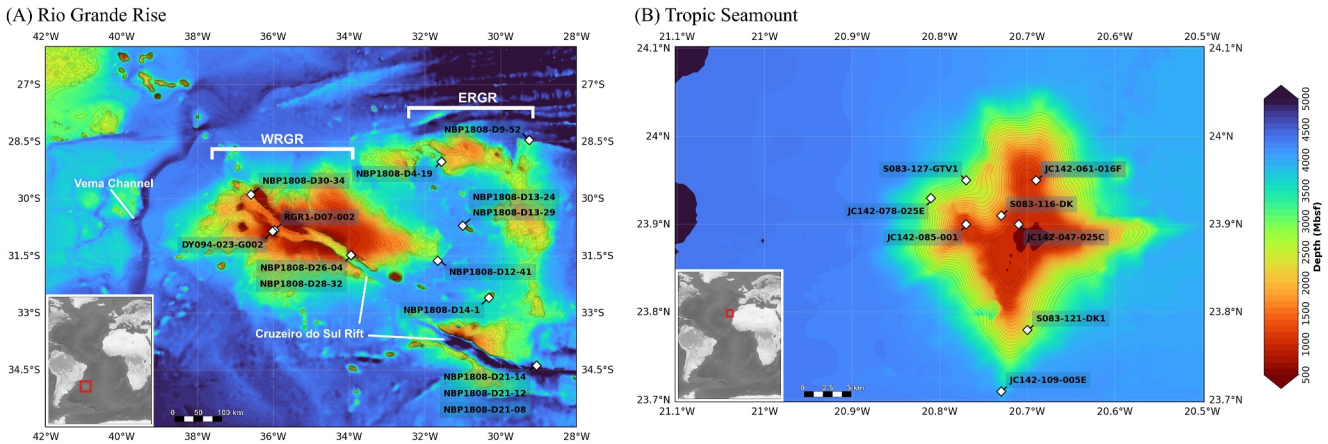

Figure 1. Bathymetric map of (a) Rio Grande Rise (RGR) and (b) Tropic Seamount (Source GEBCO) with the location of the FeMn crust samples (WRGR, Western Rio Grande Rise; ERGR, Eastern Rio Grande Rise) (Table 1).

2.2. Tropic Seamount

The TS is a part of the Canary Island Seamount Province (CISP) and is at the southwestern edge of CISP (Marino et al., 2018, 2019). TS has an area of 770 km^2. It is an isolated northeastern Atlantic volcanic edifice. It is located 400 km from West Africa's passive continental margin, halfway between the Canary Islands and the Cape Verde Islands (Figure 1). The seamount rises to a depth of 950 mbsl from the abyssal plain at 4,100 mbsl where it has a flat diamond-shaped top (Figure 1). The flanks are dominated by gullies and landslide scars separated by four spurs that radiate from the summit, exposing volcanic rocks covered by loose sediments (Palomino et al., 2016). The CISP region lies below the OMZ which extends from 100 to 700 m water depth with lowest oxygen contents between 400 and 500 m (Brandt et al., 2010, 2012).

The history of investigations on FeMn crusts from TS goes back to the 1990s. Koschinsky et al. (1996) determined an age of 12.3 Ma and an average growth rate of 3 mm/Ma based on ^{10}Be/^{9}Be dating of a 38 mm thick crust sample. By contrast, using the Co chronometer model by Manheim and Lane-Bostwick (1988), Marino et al. (2017), and (2018) calculated bulk growth rates of 1.2–1.8 mm/Ma and growth rates of 0.54–0.9 mm/Ma. Recently, Josso et al. (2019) presented an age model for FeMn crusts from TS. Their findings from the composite age projections show that there were favorable conditions from at least the Late Cretaceous (75 ± 2 Ma) for the growth of hydrogenetic FeMn deposits on the TS.

3. Materials and Methods

The samples used in this study were collected during different oceanographic expeditions. FeMn crust samples from TS were collected using the grab arm of the Remotely Operated Vehicle (ROV) *Isis* of the National Oceanography Center (Southampton, UK) during expedition JC142 on board HMRS *James Cook* in December 2016 (Josso et al., 2019). FeMn crusts samples from RGR were collected by dredging during expeditions RGR1 and DY094 on board the RV *Alpha Crucis* (Instituto Oceanografico, Universidade de São Paulo, Brazil) (Jovane et al., 2019) and HMRS *Discovery* (Benites et al., 2022) in February and October 2018, respectively. During the DY094 expedition, some FeMn crust samples were collected using the grab arm of the ROV *HyBis*. FeMn crusts from the western region (Figure 1) of RGR were dredged during the NBP1808 cruise on board the RV *Nathaniel B. Palmer* from 3 October to 12 December 2018. The 10 samples from this region that were used in this study were provided by the Marine and Geology Repository, Oregon State University, USA (Davidson et al., 2022). Samples (Figure 2) from the above-mentioned regions (Figure 1) selected for the analyses in this study are listed in Table 1.

Phosphatized and non-phosphatized hydrogenetic layers of the crust samples were sub-sampled to study the geochemical, mineralogical, and magnetic properties using different analytical techniques, as detailed below.

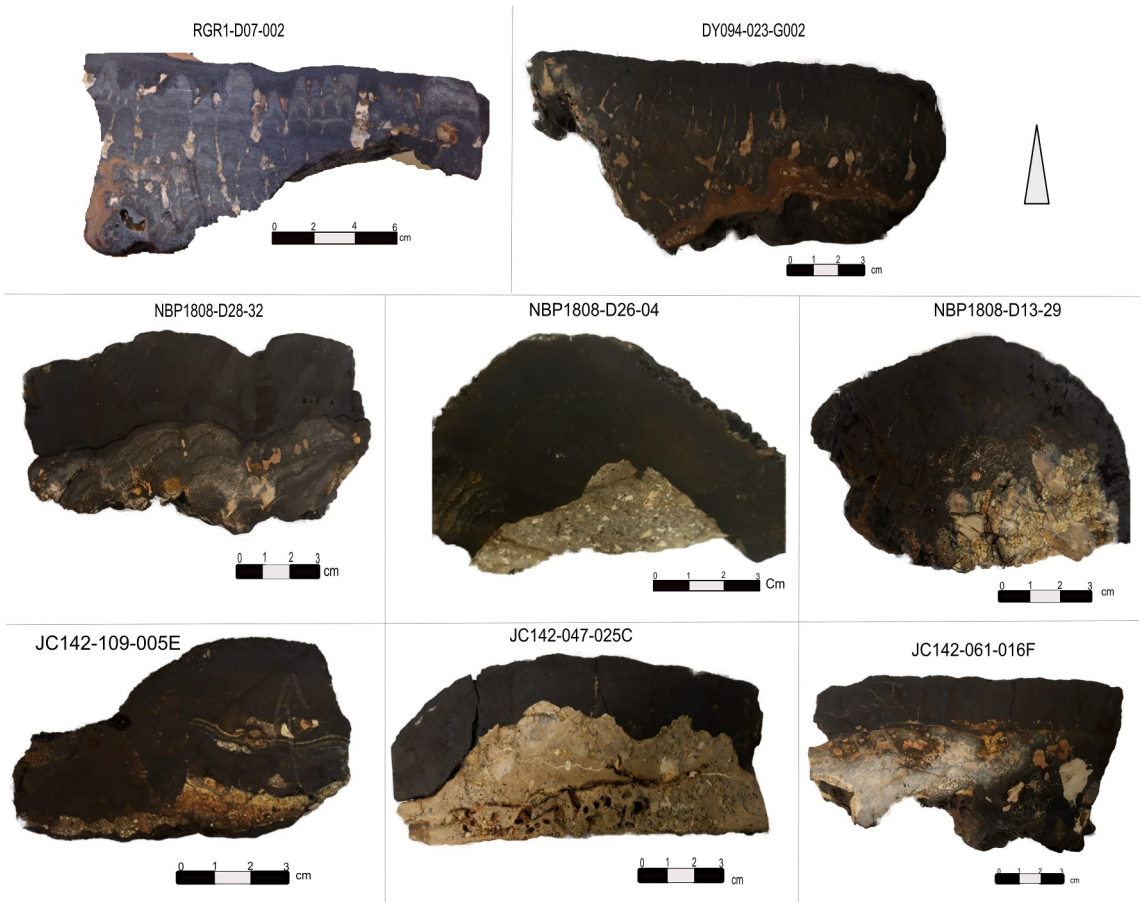

Figure 2. Photos for the hand specimens of selected FeMn crust samples from Rio Grande Rise and Tropic Seamount used for this study (details in Table 1).

3.1. Petrography, Geochemistry, and Mineralogy

3.1.1. Scanning Electron Microscopy (SEM)

SEM was performed on grain samples to understand the relationship between the texture, color and morphological features of different crust layers (i.e., fresh hydrogenetic layers and phosphatized layers) with the general grain chemistry.

The thin sections (30 μm) and slides (~1 cm) were also subjected to analyze the morphological characteristics of FeMn crusts under the MLA 650F Quanta FEG SEM (FEI Company). SEM coupled with EDS was performed at BGR, the Federal Institute for Geosciences and Natural Resources (BGR), Hannover, Germany. A high vacuum of 25 kV, a Work Distance of 10–14 mm, a spot size of 2.0–6.0 μm, and magnifications from 100X to 2,500X were used to identify different features on the FeMn crust samples.

3.1.2. Inductively Coupled Plasma Mass Spectrometry (ICP-MS) and Inductively Coupled Plasma Optical Emission Spectrometry (ICP-OES)

Major and minor elements were analyzed by using a Spectro Ciros Vision SOP ICP-OES (Inductively coupled plasma atomic emission spectroscopy) and trace elements (including the rare earth elements and high field strength elements such as Zr, Hf, Nb) were measured by Perkin_Elmer NexION 350X quadrupole ICP-MS (Inductively coupled plasma mass spectrometry) in the geochemistry laboratory at Constructor University in Bremen, Germany. All samples were carefully drilled with a micro-drill, powdered in an agate pan mill and dried at 105°C for 24 hr. Immediately after drying, 0.05 mg of each sample was digested with HCl, HNO_3 and HF in a ratio of 3:1:1 ml. Samples in the acid mixture were heated to 225°C for 12 hr in closed vessels that were later

Table 1
List of FeMn Crust Samples From Rio Grande Rise and Tropic Seamount

Sr. number	Sample name	Lat	Long	Depth (m)	Location
1	NBP1808-D21-14	−34.38	−29.06	5,218	Rio Grande Rise
2	NBP1808-D4-19	−29.02	−31.57	2,735	Rio Grande Rise
3	NBP1808-D21-12	−34.38	−29.06	5,218	Rio Grande Rise
4	NBP1808-D14-1	−32.60	−30.32	2,634	Rio Grande Rise
5	NBP1808-D21-08	−34.38	−29.06	5,218	Rio Grande Rise
6	NBP1808-D12-41	−31.62	−31.67	4,076	Rio Grande Rise
7	NBP1808-D13-24	−30.70	−31.01	2,772	Rio Grande Rise
8	NBP1808-D9-52	−28.45	−29.25	4,592	Rio Grande Rise
9	**DY094-023-G002**	**−30.82**	**−35.97**	**786**	**Rio Grande Rise**
10	NBP1808-D13-29	−30.70	−31.01	2,772	Rio Grande Rise
11	NBP1808-D26-04	−31.48	−33.95	2,190	Rio Grande Rise
12	**RGR1-D07-002**	**−30.85**	**−36.02**	**684**	**Rio Grande Rise**
13	NBP1808-D30-34	−29.89	−36.59	2,008	Rio Grande Rise
14	NBP1808-D28-32	31.47	33.95	2,190	Rio Grande Rise
15	S083-116-DK	23.91	−20.73	1,484	Tropic Seamount
16	S083-127-GTV1	23.95	−20.77	1,088	Tropic Seamount
17	S083-121-DK1	23.78	−20.70	2,377	Tropic Seamount
18	JC142-047-025C	23.90	−20.71	999	Tropic Seamount
19	JC142-061-016F	23.95	−20.69	1,122	Tropic Seamount
20	JC142-109-005E	23.71	−20.73	3,760	Tropic Seamount
21	**JC142-085-001**	**23.90**	**−20.77**	**1,130**	**Tropic Seamount**
22	**JC142-078-025E**	**23.93**	**−20.81**	**2,803**	**Tropic Seamount**

Note. Bold shows the samples used for the continuous magnetic measurements.

opened and kept at 180°C for acid evaporation. Digested samples were stored in 0.5 M HNO_3. Samples were diluted for Mn, Fe, Cu, Al, K, Ca, Mg, Na, P, V and Zn measurements using ICP-OES. Determination of Li, Sc, Ti, Co, Ni, Tl, Rb, Sr, Y, Zr, Nb, Mo, Te, Cs, Ba, REE, Hf, Ta, W, Pt, Pb, Th, and U was performed in diluted samples using ICP-MS. Certified Reference Materials (CRM) JMn-1 and Fe-Mn1 were used for precision, which was better than ±90% for most elements. To understand the oxygenation conditions for crust growth and phosphatization, REY anomalies for the phosphatized and non-phosphatized crusts were separately plotted and normalized by *Post-Archean Australian Shale (PAAS)*.

3.1.3. X-Ray Diffraction

∼1 g of powdered and oven-dried phosphatized and non-phosphatized layers of selected samples from RGR and TS were used to perform X-Ray Diffraction (XRD) measurements. Bulk samples were measured using a PANalytical X'Pert PRO MPD diffractometer Cu-kα radiation with 40 kV and 40 mA at the Federal Institute for Geosciences and Natural Resources (BGR), Hannover, Germany. The diffractometer contains a variable divergence slit and the Scientific X'Celerator detector. Samples were measured over 5°–85° with a step size of 0.0334° 2θ and a measuring time of 200 s/step. The results were processed using High Score Plus Software.

3.2. Magnetic Measurements

3.2.1. Transmission Electron Microscopy and Mössbauer Spectroscopy

The representative crust samples weighing 10 g each were gently crushed, powdered and passed through a sieve of 150 μm. To extract the magnetic particles from the powdered samples, the samples were mixed with acetate

buffer (pH 4.0) according to Strehlau et al. (2014). Samples were maintained under constant agitation overnight. Magnetic concentration using a magnet and washing steps with MilliQ were performed before sample deposition in formvar–carbon-coated grids for Transmission Electron Microscopy. Samples were observed on an FEI Tecnai Spirit (FEI Company) at 120 kV at the Instituto de Microbiologia Paulo de Góes, Universidade Federal do Rio de Janeiro.

Mössbauer spectroscopy can distinguish between ferrous and ferric iron. Magnetic particles extracted from the selected samples were also subjected to Mössbauer spectroscopy, which was carried out at the Instituto de Física, Universidade de São Paulo. Mössbauer spectroscopy was performed at room temperature using a commercial spectrometer (Wissel- Mössbauer spectrometer) equipped with a ^{57}Co source, operating in constant acceleration mode with a sampling velocity in the range of ±10 mm/s. The NORMOS software package was used to fit the obtained spectra curve by minimizing the chi-square parameter (X^2). The spectra were calibrated using metallic iron as the standard.

3.2.2. Magnetic Scanning

Magnetic scanning was performed on 1 cm thick slides of four selected samples along the growth direction of the crusts by using room temperature Hall probe magnetic microscope at the Department of Geophysics at Charles University, Prague, Czech Republic. The room-temperature instrument consisted of a stationary axial Hall probe with a sensor housed in a fiberglass tip measuring approximately 200 μm in size. A motorized 2-D stage with a spatial resolution of 1 μm was used for movement (Kletetschka et al., 2013). Among these four samples, two samples, one from RGR (RGR1-D07-002) and one from TS (JC142-085-001) were the same samples studied by Benites et al. (2020) and Josso et al. (2019). The vertical component of the magnetic field reflecting microscale magnetic direction within the sample was measured at a sensor-to-sample distance of 0.1 mm with a scanning interval of 80 μm. The scanning was repeated 100 times along the same profile. Another additional parallel profile was also measured to compare the magnetic signals. The background signal was measured without the sample which was later subtracted from the signal obtained from the crust sample. Principal Component Analysis (PCA) was performed on the normalized data separately for line A and B in each sample. While the number of extracted components varied among samples, we opted to focus on the main principal component, as it typically explained the highest percentage of variance. The remaining components generally contributed minimally to the explained variance, typically less than 1%.

3.2.3. Rock Magnetism and Paleomagnetism

Rock magnetic measurements [hysteresis cycles, First Order Reversal Curves (FORCs) and thermomagnetic curves] were performed at the CORE Lab of the IO-USP. An Alternating Gradient magnetometer Micromag 3900 from Lake Shore was used to measure the hysteresis cycles and FORCs of the subsamples collected along the FeMn crusts. Hysteresis parameters such as magnetic saturation (Ms), remanence of magnetic saturation (Mrs) and magnetic coercivity (Hc) were obtained by applying a maximum field of 1 T. FORCs were produced by applying a maximum field of 1 T, with an average time of 150 ms on 297 curves. The FORC diagrams were processed with the software "Forcot" and varying smoothing factors (SF) were applied to visualize FORC fingerprints for the measured samples (Berndt & Chang, 2019).

0.5 g of powdered crust subsamples were subjected to identify the magnetic minerals based on Curie temperature. Thermomagnetic curves are used to understand the Curie (or Neel) temperature of the magnetic minerals where magnetic susceptibility is measured at regular intervals by consecutively heating the samples. Magnetic susceptibility versus temperature curves were obtained by progressive heating and cooling in the Argon environment. Selected burnt samples were reanalyzed to understand newly formed magnetic minerals in the controlled environment. The Kappabridge MFK1 (AGICO) was used to perform the measurements. Bulk data were processed and plotted by the Cureval software provided by AGICO.

Roughly 2 mm thick slices of four FeMn crusts shown in Table 1 were cut by a cutting blade of thickness less than 0.4 mm along the growth direction of FeMn crusts as described by Yuan et al. (2017). The magnetic susceptibility of the thinly sliced samples was measured. Thinly sliced samples were also subjected to measure Natural Remanent magnetization (NRM). NRM was measured by using a 2G Enterprises Long Core Squid Magnetometer in a shielded room at the Paleomagnetic lab of the Instituto de Astronomia e Geofísica (IAG) of the Universidade de São Paulo. Stepwise Alternating Field demagnetization of 5, 10, 15, 20, 25, 30, 40, 50, 60, 70, 80, 90, and

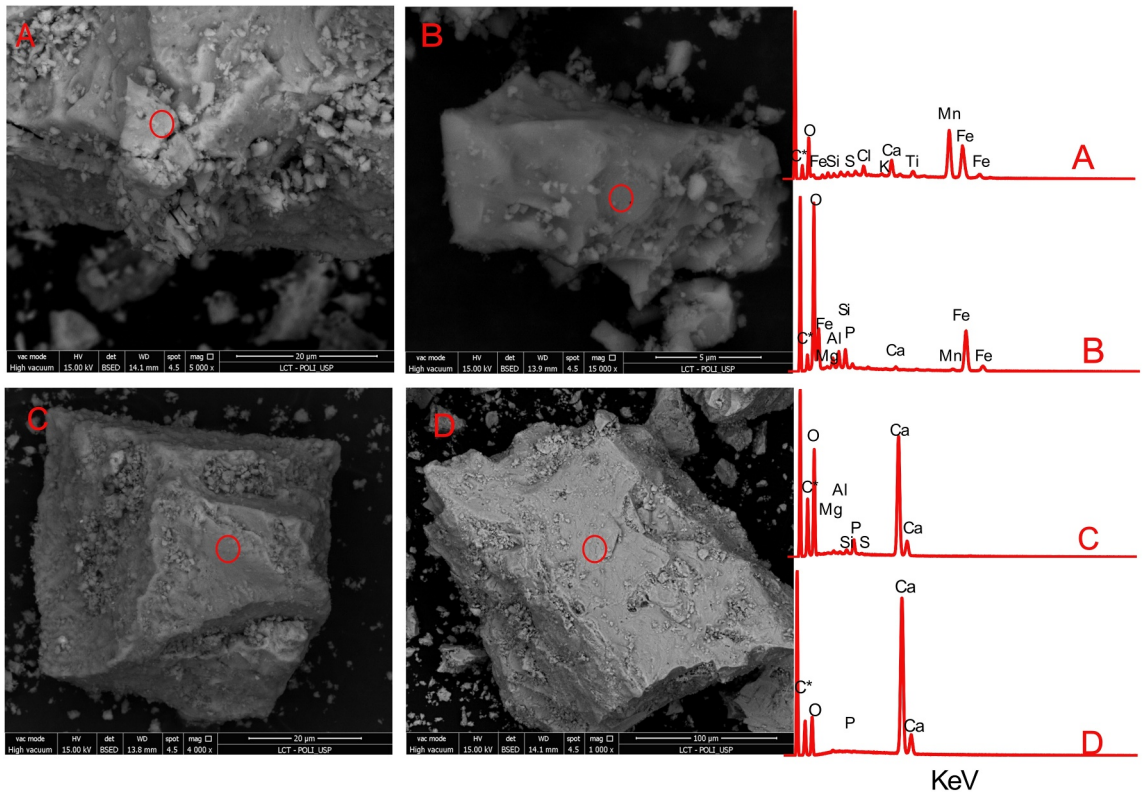

Figure 3. Scanning Electron Microscopy images of powdered samples of FeMn crusts. Circles indicate positions of EDS spectra (on the right). (a) FeMn phase from the non-phosphatized Rio Grande Rise (RGR) crust sample RGR1-D07-002, (b) FeMn phase from the non-phosphatized Tropic Seamount (TS) crust sample JC142-085-001, (c) CFA phase from phosphatized RGR crust sample RGR1-D07-002, (d) CFA phase from phosphatized TS crust sample JC142-085-001. Non-phosphatized layers are dominated by Fe and Mn oxides whereas phosphatized layers are rich in Ca and P, indicating the presence of CFA.

100 mT was employed to remove the secondary magnetic components. PuffinPlot software provided by Lurcock and Wilson (2012) was used to display the demagnetization data. PCA was performed to recognize the primary magnetic component (Characteristic Remanent Magnetization, ChRM) (Kirschvink, 1980). Samples with a Maximum Planar Deviation Angle (MAD) greater than 12° were considered unreliable.

4. Results

4.1. Petrography, Geochemistry, and Mineralogy

4.1.1. Petrography and Texture

Both in the RGR and in the TS samples, the hydrogenetic/non-phosphatized layers of the FeMn crust consist of amorphous Fe oxyhydroxide phases (Figure 3). SEM observation of thin sections revealed alternate dendritic and botryoidal textures (Figure 4). Non-phosphatized parts of FeMn crusts from TS exhibit parallel botryoidal texture while the crusts from RGR show dendritic texture (Figure 4). The phosphatized crusts are made up mainly of carbonate fluorapatite (CFA) (Figure 4). In crusts from TS the CFA accumulation occurs in fractures perpendicular to the growth direction, whereas in crusts from RGR massive and irregular accumulation of CFA occurs in pore spaces. SEM-EDS mapping of Fe, Mn, P, and Ca shows a co-occurrence of the Fe and Mn phases, whereas the abundance of CFA (shown by a high abundance of P and Ca) is negatively correlated with the abundance of Fe and Mn. This suggests that Fe and Mn phases are replaced by CFA in phosphatized crusts from both regions.

Massive ironstones are abundant and only in diagenetically altered parts of FeMn crusts from RGR (Benites et al., 2022) (Figure 4b (C)). Sample RGR1-D07-002 (RGR) (Figure 4b (G and H)) shows an Fe-rich matrix containing smooth and rounded particles, likely cosmic spherules. Cosmic spherules have been previously reported in FeMn crusts (Halbach, Kriete, et al., 1989; Halbach, Sattler, et al., 1989; Oda et al., 2018; Savelyev et al., 2022). Samples from both regions also contain volcanic breccia cemented by CFA in the phosphatized

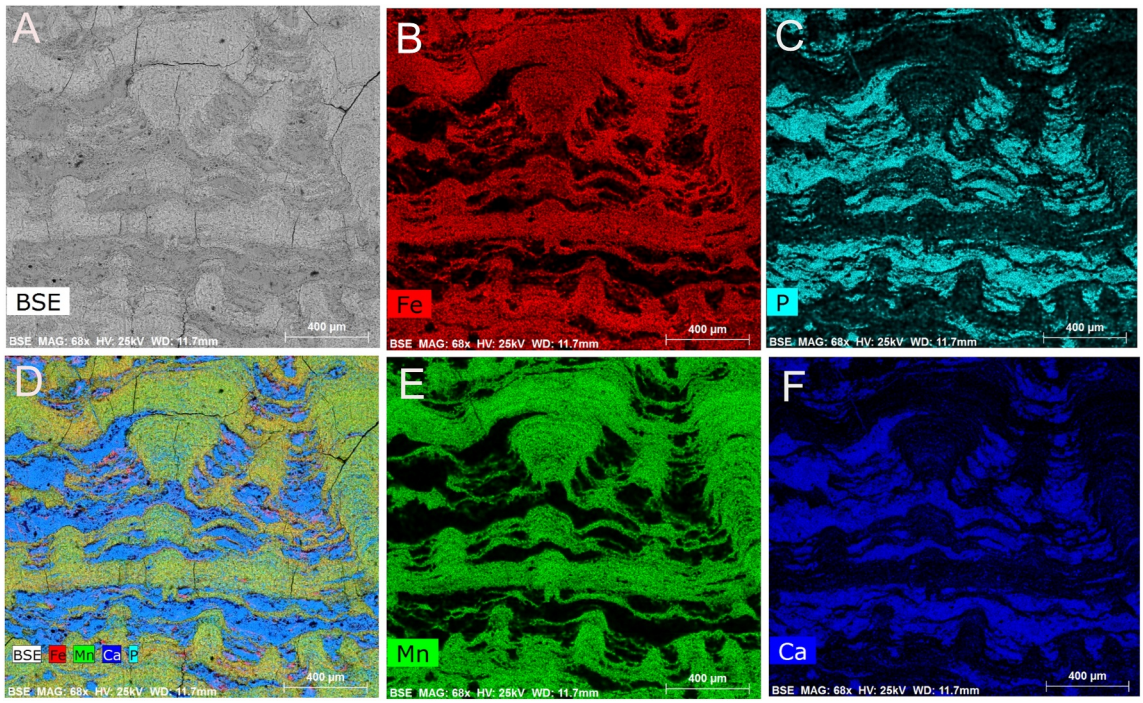

Figure 4. (a) Scanning Electron Microscopy (SEM) image (BSE = Backscattered Electron) and EDS maps of Fe, Mn, Ca, and P in a thin section of FeMn crust sample DY094-023-G002 (Rio Grande Rise (RGR)). Fe and Mn-rich layers are depleted in P and Ca, suggesting the replacement of FeMn layers by CFA. D is the composite image of A, B, C, E, and F. (b) SEM images of FeMn crusts: (A–C): DY094-023-G002 (RGR), (A) Backscatter Electron (BSE) image of typical hydrogenetic FeMn layers, (B) EDS elemental mapping of the phosphatized crust showing the dendritic texture filled with foraminifera enriched CFA, (C) EDS elemental mapping of the phosphatized crust showing massive ironstone texture (dark red); (D–F) JC142-085-001 (Tropic Seamount), (D) Fe-rich grain being replaced by CFA, (E) Fracture filled by CFA, (F) CFA filling pore space; (G–I) RGR1-D07-002 (RGR), (G) BSE image of smooth and circular cosmic spherules inside a Fe-rich matrix, (H) EDS elemental mapping of the spherule-rich area, (I) Bacterial mats with CFA crystals.

layers of the crusts, which have also been previously reported (Benites et al., 2022; Marino et al., 2019; Staszak et al., 2022; Varentsov et al., 1991).

4.1.2. Geochemistry

ICP-OES data were used to build ternary and binary diagrams from Bonatti et al. (1972) and Dymond et al. (1984). Both diagrams are based on the concentration of Fe, Mn, Co, Ni, and Cu in each subsample (non-phosphatized or phosphatized). The data plotted in both diagrams suggest that all the studied crusts from both regions formed hydrogenetically (Figure 5).

ICP-MS data (Figures 6 and 7) separate non-phosphatized from phosphatized crusts, as positive cerium and negative yttrium anomalies are diagnostic for non-phosphatized crusts, indicating oxic environment for the growth of the younger layers (Bau et al., 2014). A positive yttrium anomaly is common for phosphatized crusts (Figure 7); however, the cerium anomalies are negative in some samples and positive in others, indicating a suboxic environment for the phosphatization of the crusts (Bau et al., 2014). REY are enriched in phosphatized crusts from both regions (Figure 7). Some phosphatized samples have undergone intense phosphatization, especially in brecciated parts of the phosphatized layers showing a very negative cerium anomaly (Figure 7). Our results are consistent with previous studies (Bau et al., 2014; Benites et al., 2022; Koschinsky et al., 1997; Kuhn et al., 1998; Sousa et al., 2021). Jiang, Sun, et al. (2020) and Jiang, Zhao, et al. (2020) studied phosphatized FeMn crusts in which different stages of phosphatization corresponded to different intensities of negative cerium anomaly. The binary diagram of Bau et al. (2014) identifies the quadrant of hydrogenetic FeMn crusts based on Ce_{SN}/Ce_{SN}^* versus Nd and Y_{SN}/Ho_{SN}. Most of the non-phosphatized samples used in this study fall into the hydrogenetic field (Figure 6). Although Bau et al. (2014) pointed out that this classification should not be used for phosphatized crusts, we also plotted the phosphatized samples in the diagram to stress the separation of phosphatized and non-phosphatized crusts (Figure 6).

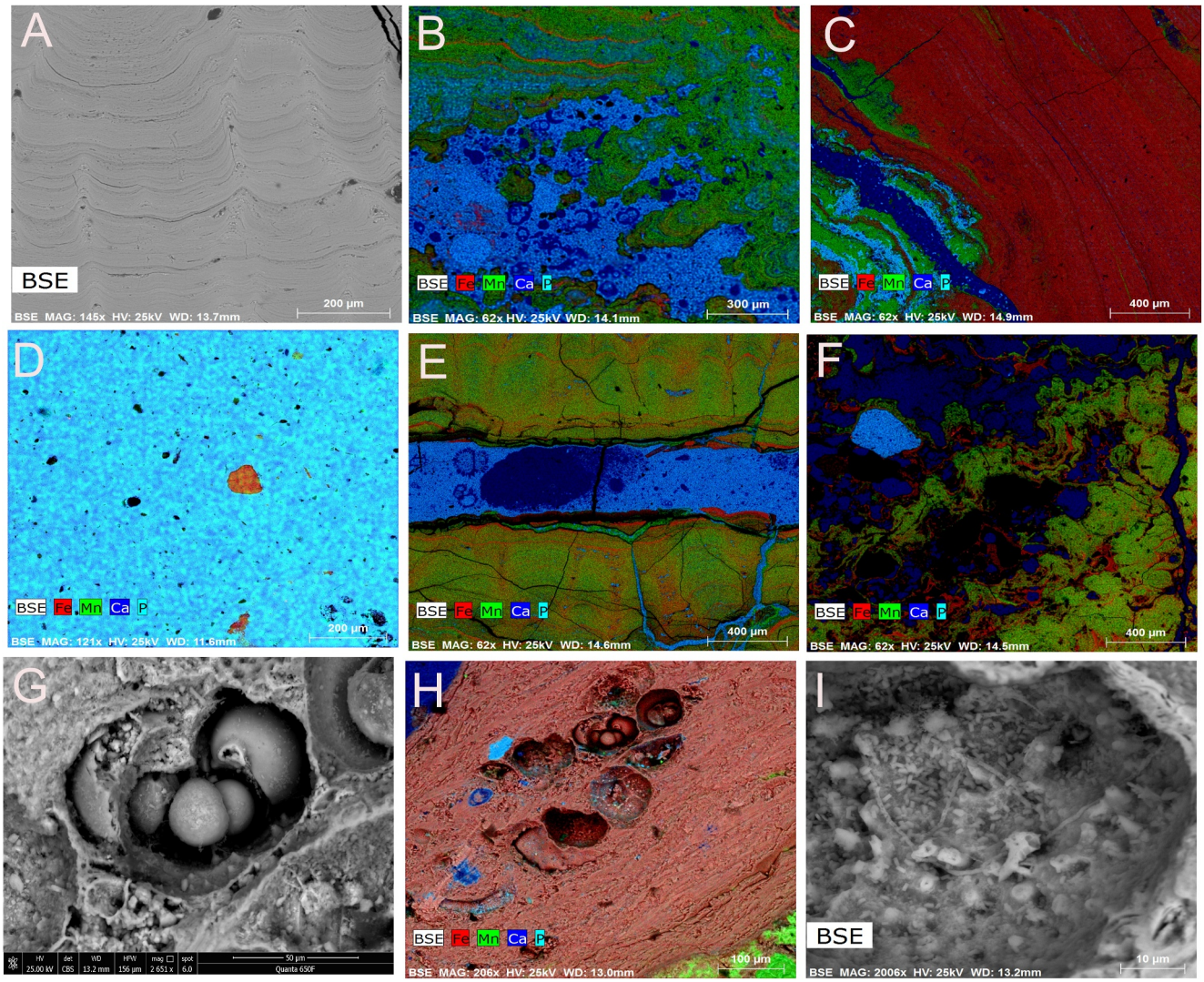

Figure 4. (Continued)

Elemental ratios of Fe, Mn, Ca, and P in phosphatized and non-phosphatized crusts (Figure S1 in Supporting Information S1) suggest that phosphatization causes the removal of Fe-oxyhydroxides while increasing the abundance of CFA. This process not only removes magnetic components but also increases the diamagnetic dilution of remaining magnetic signals in the phosphatized crusts. Both the geochemical classifications and the REY content show that hydrogenetic and phosphatized crusts are geochemically distinct. Phosphatization occurred in suboxic conditions, which led to replacement of Fe and Mn oxyhydroxide phases.

4.1.3. Mineralogy

XRD results show that the hydrogenetic FeMn crusts contain amorphous Fe-oxyhydroxides and Mn-oxides, whereas the crystalline phases are vernadite with traces of quartz and calcite (Figure 8). The phosphatized crusts exhibit a higher variety and abundance of minerals relative to non-phosphatized crusts, including todorokite, apatite, feldspar, vernadite, calcite and goethite. The different mineral associations in non-phosphatized and phosphatized FeMn crusts suggest formation in different oceanographic conditions. The volcanic breccia cemented by CFA showing distinct negative Cerium anomalies (Figure 7) contains minerals that are common in phosphatized crusts, plus the presence of significant amount of magnetic minerals detectable by XRD (i.e., magnetite/hematite) (Figure 8).

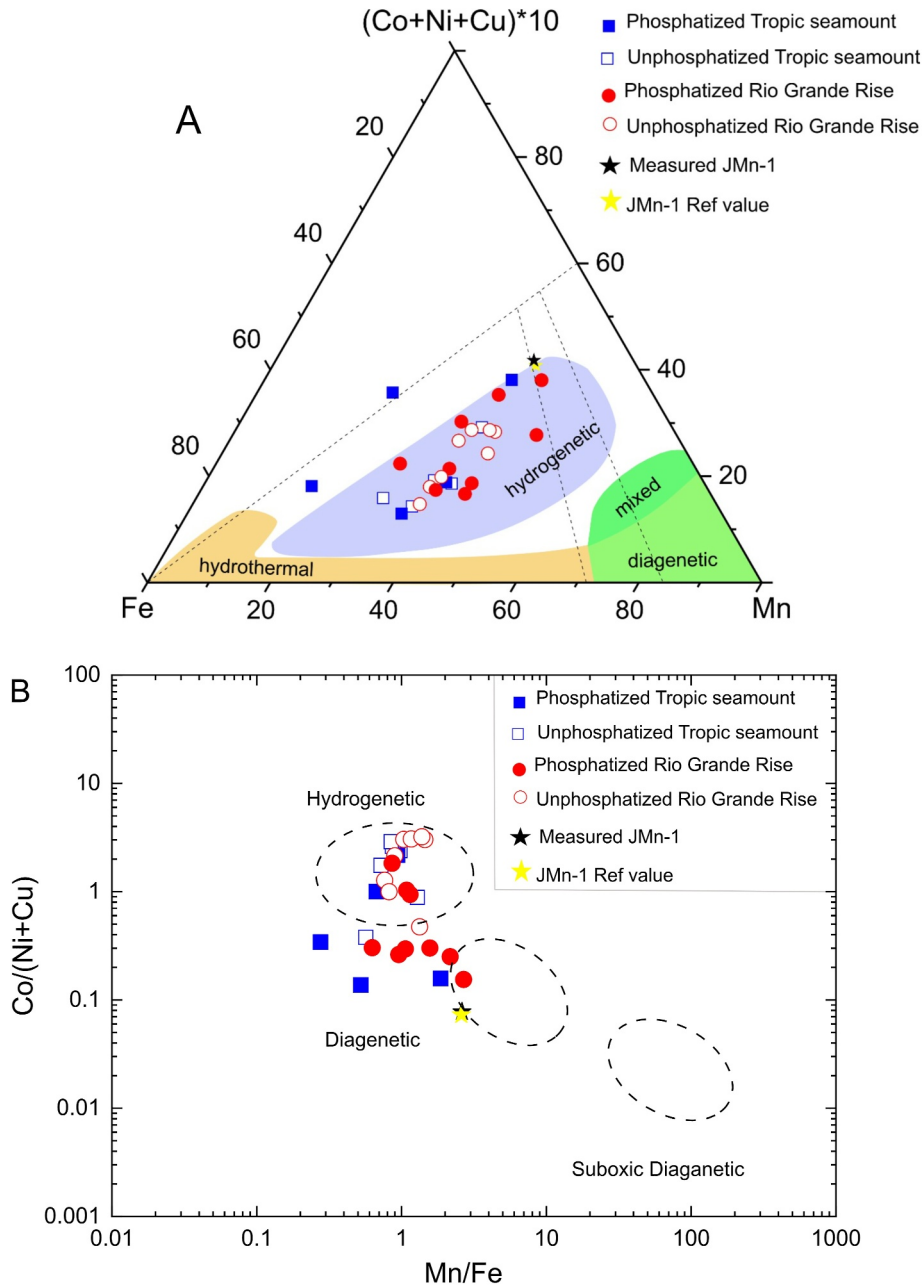

Figure 5. Ternary and binary diagrams: (left) The ternary diagram by Bonatti et al. (1972) and (right) Binary diagram by Dymond et al. (1984). Both diagrams classify the studied samples as hydrogenetic FeMn crusts. JMn-1 indicates the certified reference material (CRM) prepared by the Geological Survey of Japan (Terashima et al., 1995).

4.2. Magnetism

4.2.1. Rock Magnetism and Paleomagnetism

In general, rock magnetic measurements on non-phosphatized layers of the FeMn crust samples from both regions show the presence of paramagnetic/superparamagnetic. The hysteresis loops reveal very low coercivity values, while the corresponding FORCs display interaction among nanoparticle indicating the absence of single domain non-interacting magnetic component for the non-phosphatized layers of FeMn crusts.

The hysteresis curves of phosphatized subsamples from RGR and TS exhibit characteristic features associated with high coercivity minerals as these samples don't saturate at the maximum applied magnetic field. FORCs also

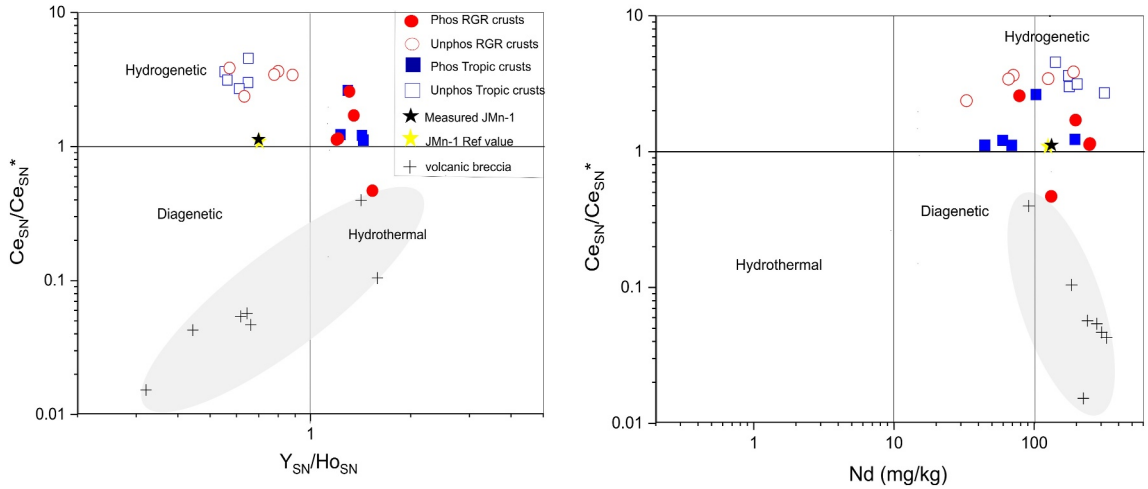

Figure 6. Binary diagrams from Bau et al. (2014)—Ce_{SN}/Ce_{SN}* versus Nd and Y_{SN}/Ho_{SN} classify hydrogenetic, hydrothermal and diagenetic FeMn crusts, based on Y, Hoand Nd contents. The shaded area of the binary diagram represents the highly altered brecciated parts (volcanic breccia) of FeMn crusts from both Rio Grande Rise and Tropic Seamount (Ce, Cerium; Nd, Neodymium; Y, Yttrium; Ho, Holmium; SN, Shale-normalized).

indicate the presence of a high coercivity magnetic component for these samples (see Figure 9a). The hysteresis loops and FORCs from the phosphatized sections containing volcanic breccia from both regions depict a low coercivity pseudo-single domain ferromagnetic fraction with superparamagnetic components (Figure 9b).

Fittings with two doublets from the Mössbauer spectra reveal that there are no magnetic Fe oxides since sextets do not appear (Figure 11). The values of the isomeric shifts relative to metallic Fe are (0.31, 0.48) for RGR1-D07-002 (RGR) and (0.30, 0.49) for JC142-085-001 (TS) and (0.24, 0.42) for JC-142-078-025E (TS). These isomer shift values are all characteristic of Fe^{3+} oxidation states. Mössbauer spectroscopy revealed no Fe^{+2} in the magnetic extract. Our results are consistent with previous studies on FeMn nodules and crusts from the Indian Ocean (Carpenter & Wakeham, 1973; Ganwani et al., 2017; Pattan & Mudholkar, 1991; Rusanov et al., 2008).

FeMn crust slices used for the stepwise demagnetization showed no signs of smooth demagnetization and hence the results would not show reliable ChRM (Figure S3 in Supporting Information S1). Most of the samples resulted in MAD 3 angle greater than 12° providing vague and ambiguous results.

4.2.2. Magnetic Scanning

Hall probe magnetic scanning performed on four crust samples suggests the FeMn crusts from RGR and TS don't show primary remanence characteristics. The scanning lines A and B (Figure 12a (except 62–102 mm) and Figure 12b) exhibit considerable similarity, indicating a high level of accuracy in the measured magnetic signal. However, scanning lines A and B (Figure S4a in Supporting Information S1) display notable differences with very low values, whereas scanning lines A and B (Figure S4b in Supporting Information S1) illustrates similarity between lines A and B. In all samples, the magnetic data obtained from Hall probe scanning is not consistent with the expected variation in magnetic intensity, consequently confirming that the studied FeMn crusts don't show signs of original magnetic remanence. The samples (Figure S4a (TS) and Figure S4b (RGR) in Supporting Information S1) are already dated by using radioisotopes (Benites et al., 2020; Josso et al., 2019). Change in magnetic data is caused by the variation in geochemistry and mineralogy as the magnetic changes correlate with the concentration of Fe and P. This implies that the magnetic minerals have suffered diagenetic alteration during phosphatization under sub-oxic conditions, causing the complete disappearance of primary remanent magnetization. Suboxic dissolution of magnetic minerals especially biogenic magnetite has been well explained in previous studies (Karlin, 1990; Maxbauer et al., 2016; Roberts, 2015; Xu et al., 2020; Yamazaki, 2020).

Acicular goethite in some layers of crust samples is a result of continental detritus (Josso et al., 2019), whereas crust samples from RGR show the crystallization of goethite in the form of "ironstone" in the diagenetically altered (phosphatized) layer (Benites et al., 2020). According to Benites et al. (2022), goethite started

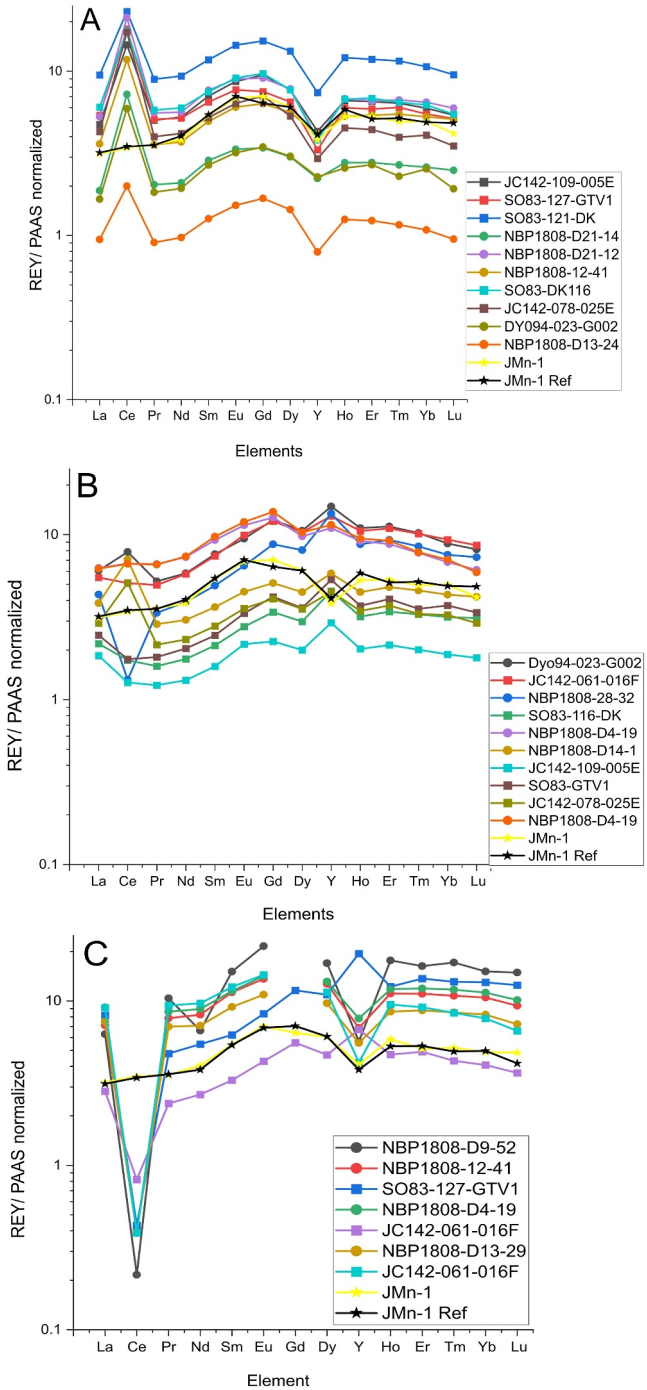

Figure 7. Shale normalized, Rare Earth Elements and Yttrium: (a) Hydrogenetic non-phosphatized FeMn crusts showing negative yttrium and positive cerium anomalies, (b) Phosphatized crusts showing positive yttrium anomaly and significantly smaller Ce anomalies compared to (a), (c) Highly altered brecciated parts of FeMn crusts with very negative cerium anomaly. Yellow and black lines in (a–c) show the standard CRM JMn-1.

mineralizing from the late Miocene extending to the Quaternary due to the several generations of bacterial mats and Fe dissolution and reprecipitation.

5. Discussion

Marine magnetic anomaly data have been previously described for the characterization of rocks in the RGR (Sergipe et al., 2023). Despite widespread pavements of FeMn crusts have been previously reported in the region (Benites et al., 2020, 2022; Jovane et al., 2019; Sousa et al., 2021), FeMn crusts do not show any significant magnetic anomaly, as their magnetic signals are almost indistinguishable from the background (Sergipe et al., 2023). To explain the absence of magnetic anomaly, we propose that the absence of remanence-carrying magnetic minerals and the presence of X-ray amorphous, weakly magnetic (paramagnetic and superparamagnetic) Fe-oxyhydroxides provide more convincing arguments than the effects of erosion and the reduced thickness of FeMn crusts, proposed by Sergipe et al. (2023).

Hydrogenetic/non-phosphatized FeMn crusts contain abundant, poorly crystalline, X-ray amorphous Fe oxyhydroxides and intergrown minerals, such as vernadite (Benites et al., 2022; Josso et al., 2019; Marino et al., 2017, 2019). Hysteresis loops and FORCs indicate that the predominant magnetic fractions of non-phosphatized layer for FeMn crusts from both RGR and TS consist of paramagnetic and superparamagnetic signatures suggesting the presence of amorphous goethite in the non-phosphatized layers (Figure 9). Whereas those for the phosphatized layer consist of vague signatures for non-interacting single domain high coercivity magnetic minerals suggesting the presence of poorly crystalline goethite in the phosphatized layers (Figure 9). The presence of acicular goethite was also confirmed in TEM images (Figure S2 in Supporting Information S1). Thermomagnetic curves during second heating showed the presence of goethite (Figures 10e and 10f), which was to confirm that the Fe containing magnetic material in the original sample is amorphous Fe oxyhydroxides. In the second heating process, the Fe and hydroxyl ions got time to arrange themselves to form crystallized Fe oxyhydroxide (goethite). This implies that, although FeMn crusts are rich in Fe, they do not contain remanence-carrying crystalline magnetic minerals. Only Fe(III) is present in the crusts (Figure 11), in line with previous studies pointing out that Fe(III) dominates amorphous and poorly crystalline Fe oxides and Fe oxyhydroxides (Carpenter & Wakeham, 1973; Ganwani et al., 2017; Murad & Schwertmann, 1988; Pattan & Mudholkar, 1991; Rusanov et al., 2008).

Previous magnetostratigraphic studies on FeMn crust from the Pacific Ocean, China Sea and Indian Ocean were based on the concept that primary remanent magnetization arises from biogenic magnetite produced by magnetotactic bacteria or detrital magnetite (Noguchi, Oda, et al., 2017; Noguchi, Yamamoto, et al., 2017; Oda et al., 2011; Yuan et al., 2017). However, there is still no compelling explanation of the mechanism of magnetite biomineralization or of the preservation of detrital magnetite in hydrogenetic FeMn crusts on a global scale.

Yuan et al. (2020) proposed that the precipitation of hydrogenetic FeMn crusts is an inorganic colloidal process that consumes oxygen and forms a protective layer between the oxygenated deep water and the FeMn phase, promoting suitable conditions for the biomineralization of magnetic minerals. According to these authors, the corrosion and dissolution of fine plankton particles would cause a decrease in oxygen concentration, promoting a microaerophilic environment suitable for

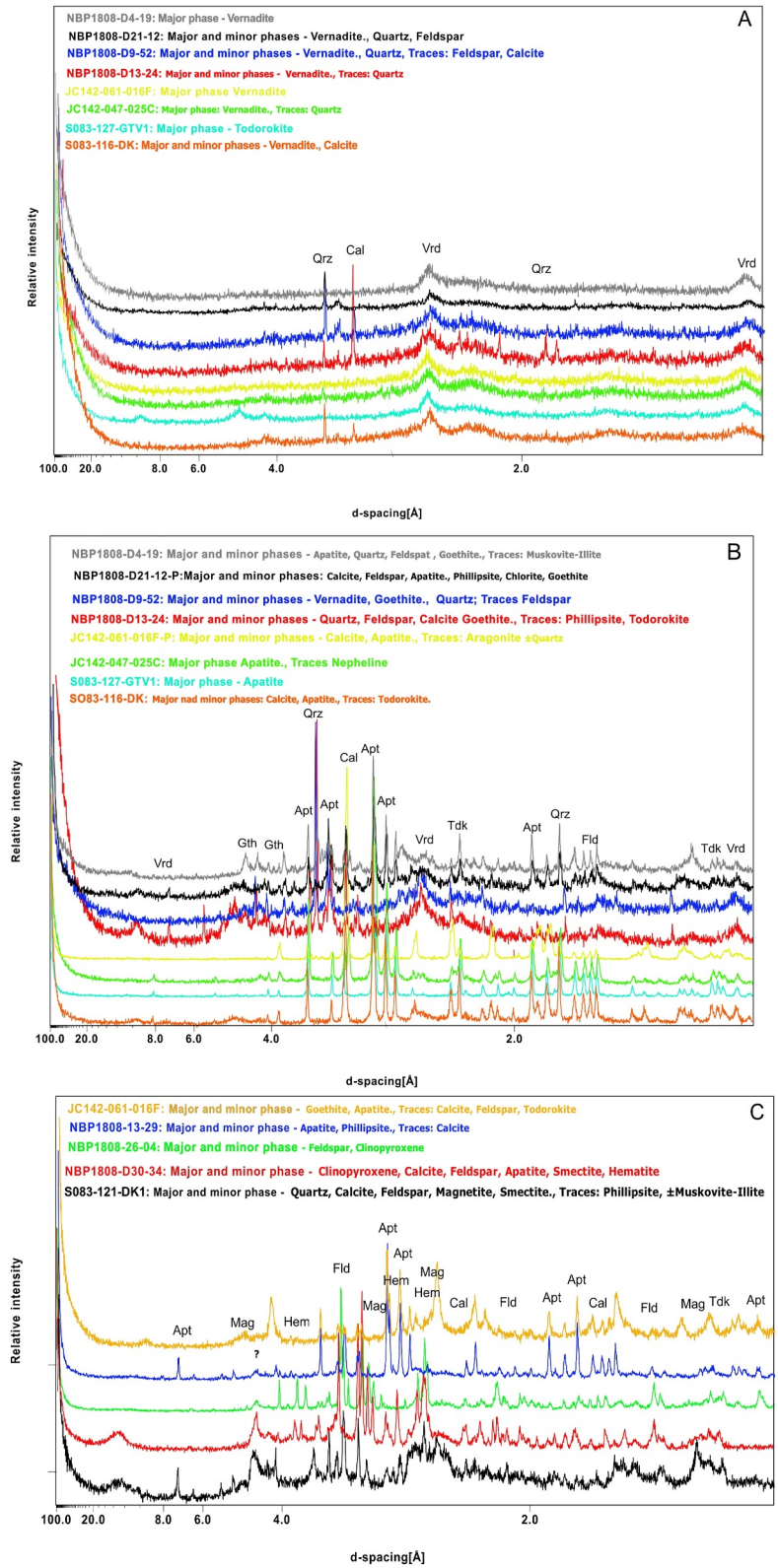

Figure 8. X-Ray Diffraction results: (a) Hydrogenetic non-phosphatized FeMn crusts showing the presence of vernadite, quartz and calcite, (b) Phosphatized crusts showing a variety of minerals including apatite, feldspar, quartz, calcite, todorokite, vernadite and goethite, (c) Phosphatized crusts with volcanic breccia containing magnetic minerals (Vrd, Vernadite; Qrz, Quartz; Cal, Calcite; Gth, Goethite; Tdk, Todorokite; Apt, Apatite; Mag, magnetite; Hem, Hematite; Fld, Feldspar; Cal, Calcite).

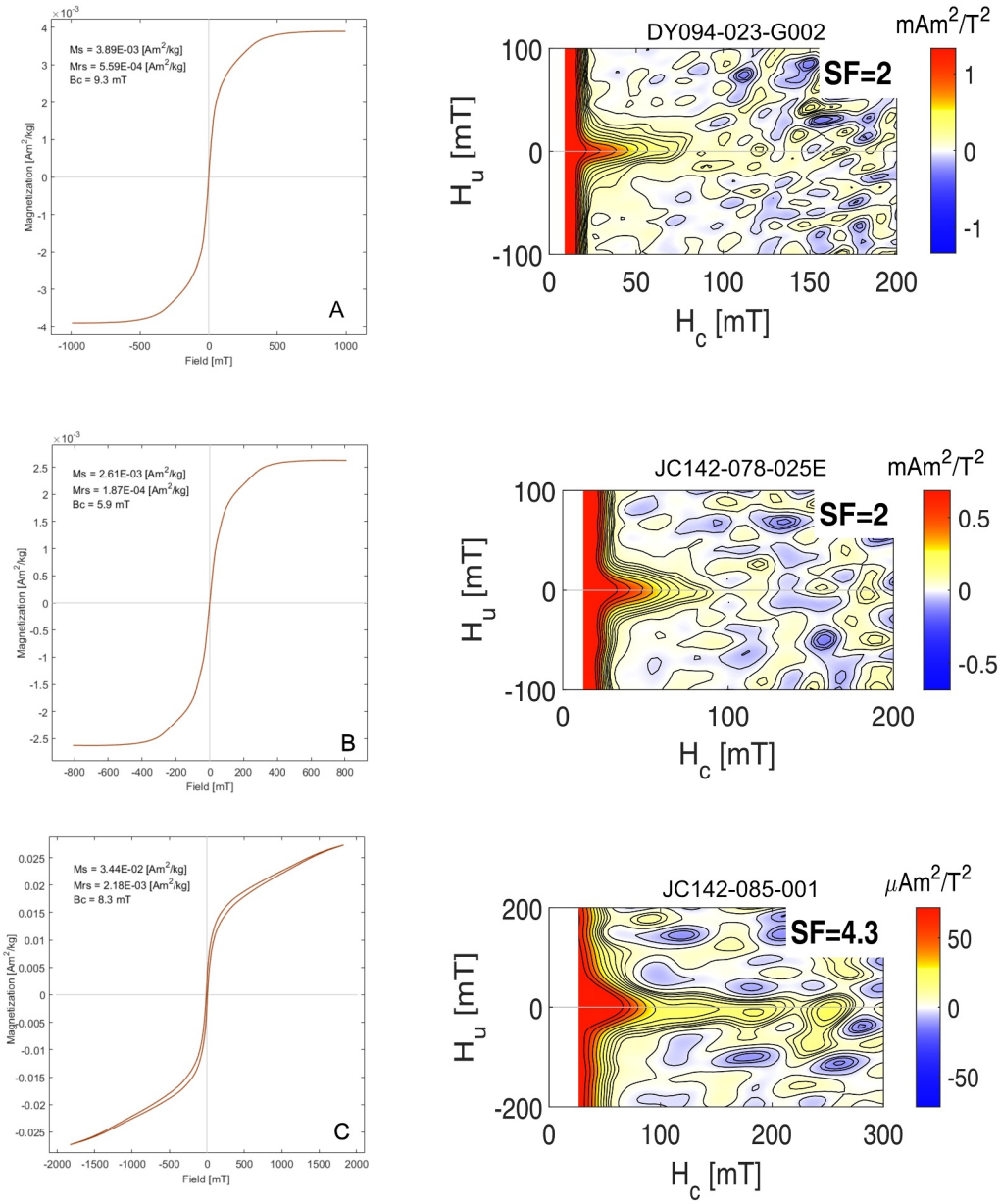

Figure 9. (a) Hysteresis loops and corresponding First Order Reversal Curves (FORCs): (A) Hysteresis loop and FORCs for the non-phosphatized layer of FeMn crust from the Rio Grande Rise (RGR), representing paramagnetic/superparamagnetic amorphous Fe oxyhydroxides (B) Hysteresis loop and FORCs for the non-phosphatized layer of FeMn crust from the Tropic Seamount (TS), representing paramagnetic/superparamagnetic amorphous Fe oxyhydroxides (C) Hysteresis loop and FORCs for the phosphatized layer of FeMn crust from the RGR, representing poorly crystalline Goethite, (D) Hysteresis loop and FORCs for the phosphatized layer of FeMn crust from the TS, representing poorly crystalline goethite (The hysteresis loops are not open probably showing the magnetic characteristics of Fe ion in paramagnetic and superparamagnetic form). (b) Hysteresis loops and corresponding FORCs: (E) Hysteresis loop and FORCs for the phosphatized volcanic breccia of FeMn crust from the RGR, representing low coercive pseudo-single domain ferromagnetic fraction with superparamagnetic components, (F) Hysteresis loop and FORCs for the phosphatized volcanic breccia of FeMn crust from the TS, representing low coercive pseudo-single domain ferromagnetic fraction with superparamagnetic components.

magnetotactic bacteria (Yuan et al., 2020). Our studies show no evidence of magnetotactic bacteria (MTB) in the studied FeMn crust, hence the magnetite biomineralization in FeMn crusts could be a local rather than a regional or global phenomenon of primary biogeochemical remanent magnetization, depending on the local availability of oxygen and organic matter. Moreover, oscillating microenvironmental conditions could lead to magnetite dissolution under suboxic conditions or magnetite oxidation under oxic conditions, raising the question about the

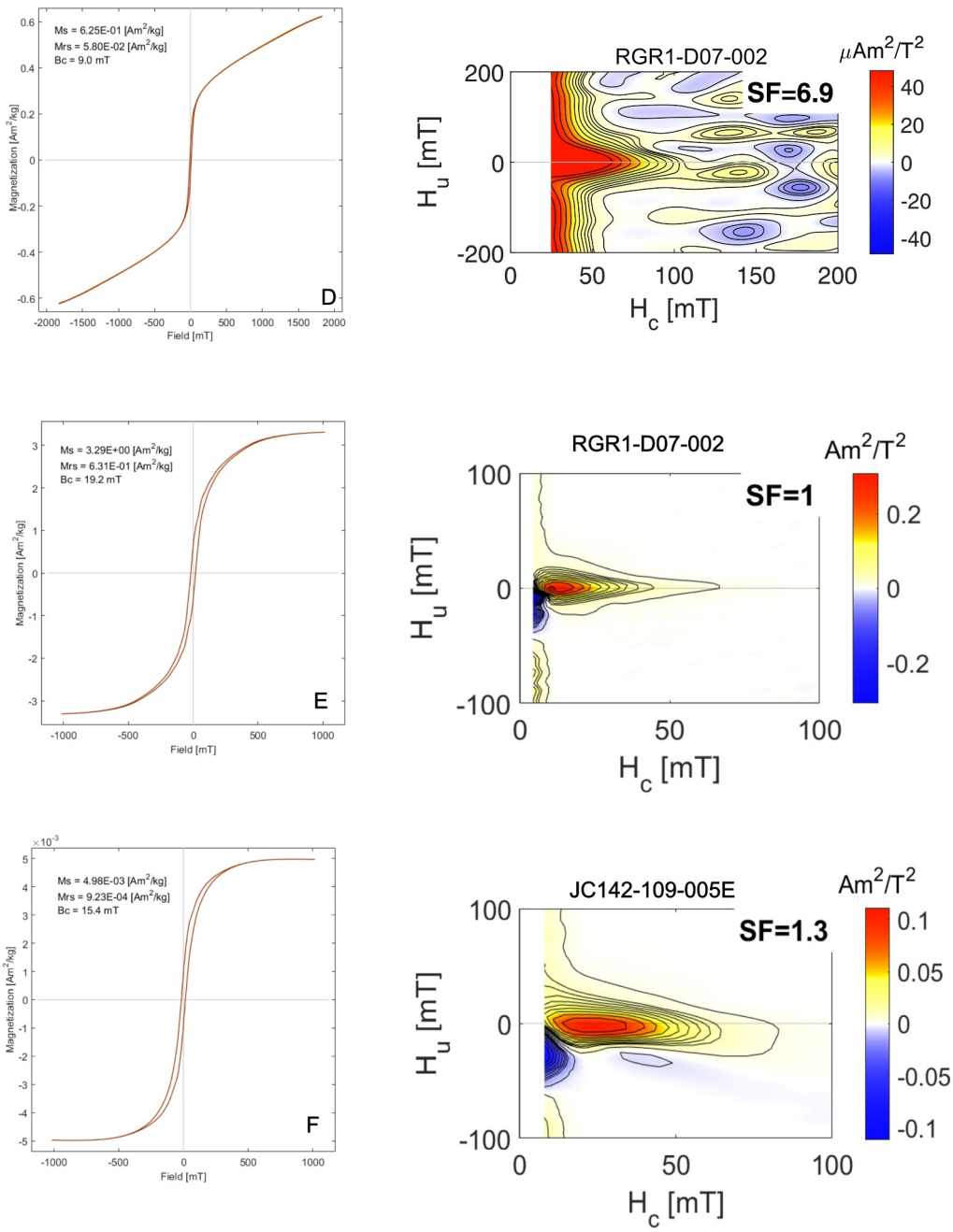

Figure 9. (Continued)

stability of biogenic magnetite both in hydrogenetic and diagenetic (phosphatized) FeMn layers. In other words, if biogenic magnetite was a primary magnetic mineral in FeMn crusts, it would probably be rapidly oxidized to Fe (III) (Liu et al., 2012; Stumm et al., 1996), generating poorly crystalline Fe oxyhydroxides. Biogenic magnetite is stable only under a narrow range of redox and pH conditions (Bazylinski & Frankel, 2004; Faivre & Schuler, 2008; Kopp & Kirschvink, 2008; Rodelli et al., 2018, 2019). In oxygenated environments, biogenic magnetite is expected to oxidize, whereas, in suboxic environments, it is expected to dissolve (Faivre & Schuler, 2008; Kopp & Kirschvink, 2008; Roberts et al., 2011; Rodelli et al., 2018, 2019). Biogenic magnetite is stable in the oxic-suboxic transition zone where oxygen is controlled by MTB (Yamazaki & Ikehara, 2012). Remanence-

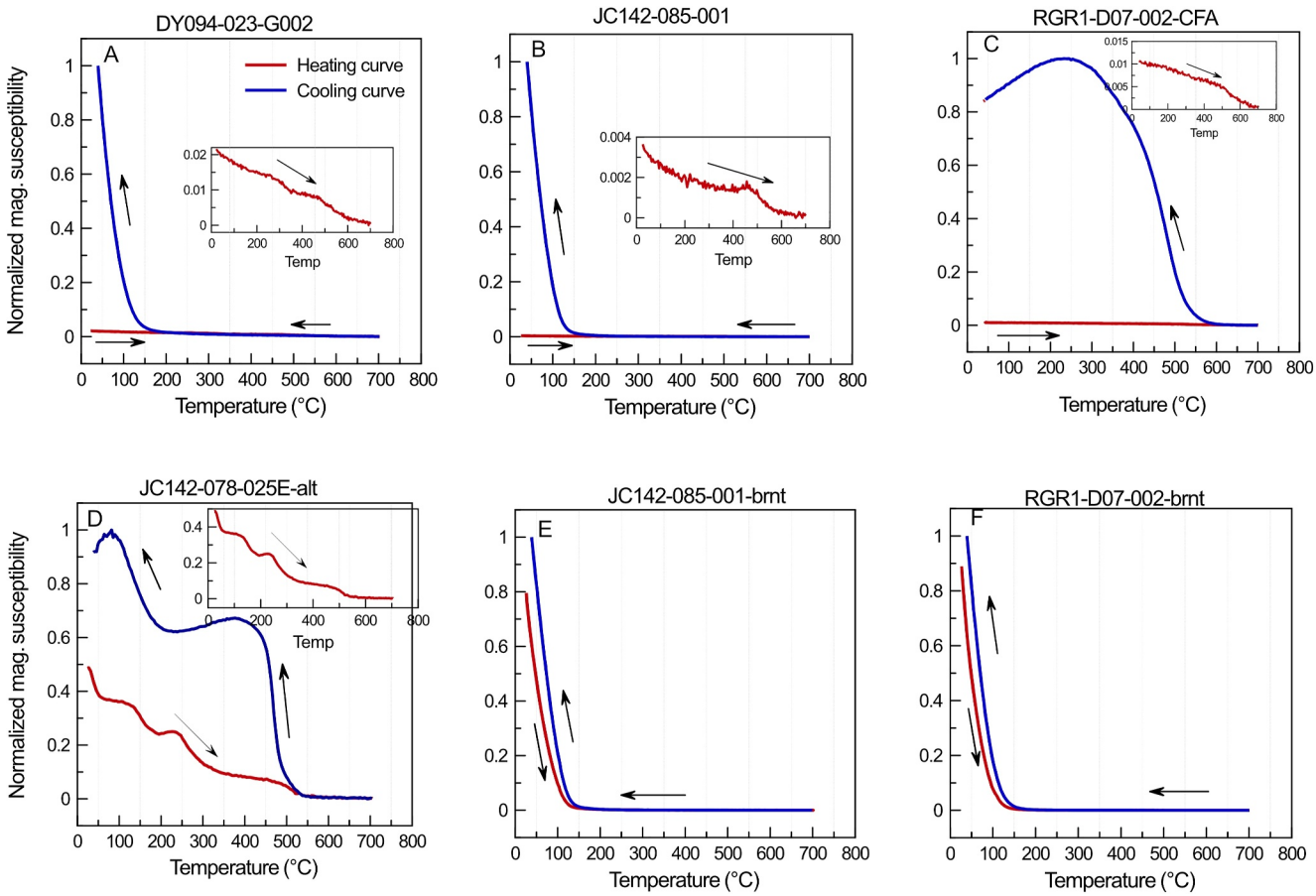

Figure 10. Thermomagnetic curves for: (a) Non-phosphatized sample from Rio Grande Rise (RGR), (b) Non-phosphatized sample from Tropic Seamount (TS), (c) Phosphatized sample from RGR, (d) Phosphatized sample from TS, (e) Remeasurement of already analyzed sample (TS) in the Argon environment, representing goethite with the Curie temperature at 120°C, (f) Remeasurement of already analyzed sample (RGR) in the Argon environment, representing goethite with the Curie temperature at 120°C.

carrying magnetic minerals have not been found either in the non-phosphatized or in the phosphatized layers of FeMn crusts presented in this study. However, hematite and magnetite are present in some samples containing volcanic breccia (Figure 8). Our samples do not contain stable ferromagnetic Fe oxides and, to the best of our knowledge, no studies have described the formation of well-crystallized Fe oxides (other than biogenic magnetite) in FeMn crusts. However, amorphous Fe oxides have been previously reported by Guan et al. (2017). Oxidation of pre-existing minerals should be considered a common phenomenon because hydrogenetic non-phosphatized crusts normally grow under oxic conditions (e.g., Marino et al., 2017), which is evidenced by the pronounced positive cerium anomaly (Figure 7). A metal-rich OMZ above the top of seamounts can serve as a metal source for the formation of FeMn crusts. However, these metals get oxidized before precipitation on the substrate (Marino et al., 2017). The oxidation of dissolved Fe(II) is the major cause of the absence of crystallized ferrimagnetic minerals. Furthermore, the biogenic oxidation of reduced forms of Fe and Mn by microbial communities has been pointed out as the earliest stage of FeMn formation (Jiang et al., 2019; Templeton et al., 2009).

We propose a model for the formation of well-crystallized Fe oxides, especially biogenic magnetite, in non-phosphatized FeMn crusts, as illustrated in Figure 13. The formation of FeMn crusts near the OMZ can be the cause for the formation of biogenic magnetite. In line with Larrasoaña et al. (2014) and Yuan et al. (2020), we propose that remanent magnetization is linked to biogenic magnetite produced by magnetotactic bacteria. Magnetite preservation is favored in a microaerophilic environment due to the decomposition of organic matter. Biogenic magnetite preservation is favored, especially on the top of seamounts directly below the OMZ. Changes in the depth of the OMZ through time, can influence the preservation of remanence-carrying Fe oxides.

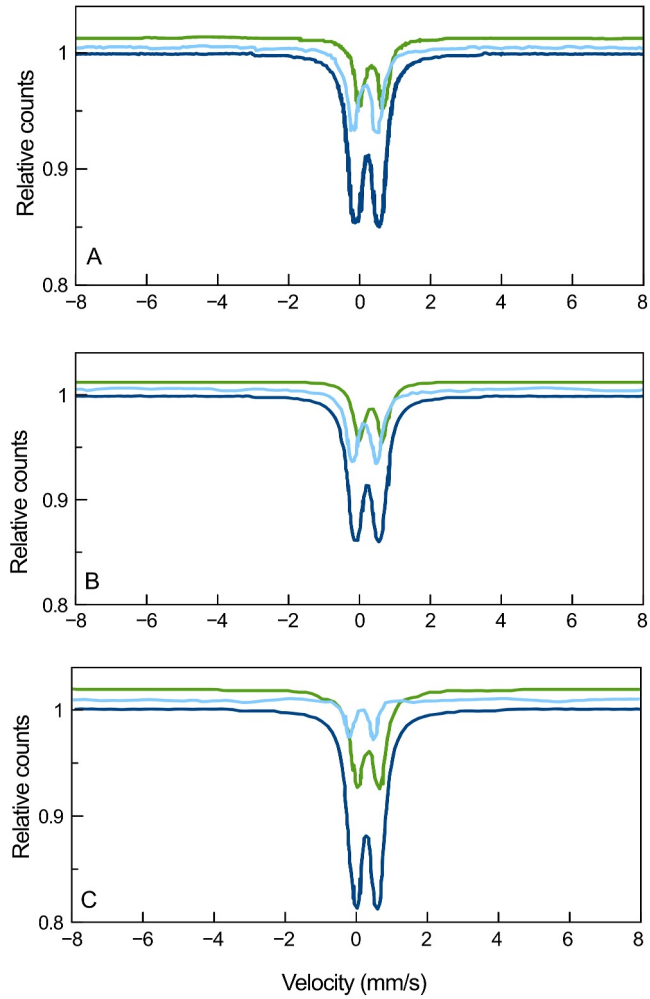

Figure 11. Mössbauer Spectroscopy of magnetic extract: (a) Non-phosphatized sample with amorphous Fe oxyhydroxides from Rio Grande Rise (RGR1-D07-002), Isomeric shift relative to metallic Fe is 0.31, 0.48, representing Fe^{+3} phase (b) Non-phosphatized sample with amorphous Fe oxyhydroxides from Tropic Seamount (TS) (JC142-085-001), Isomeric shift relative to metallic Fe is (0.30, 0.49), representing Fe^{+3} phase (c) Phosphatized sample with abundant poorly crystalline goethite from TS (JC142-085-001), Isomeric shift relative to metallic Fe is (0.24, 0.42) representing Fe^{+3} phase only.

The phosphatization of FeMn crusts is linked to oceanic circulation overturning due to the upwelling of nutrients promoted by increased biological productivity (Halbach & Puteanus, 1984). As a result, a phosphate-rich OMZ may extend to the seamount summit where FeMn crusts grow. Phosphate-rich suboxic water causes dissolution and diagenetic alterations of FeMn crusts. Since FeMn crusts are highly porous (Hein et al., 2000), these diagenetic alterations initiate the impregnation and replacement of FeMn phase by the CFA, initially by precipitating minerals such as todorokite (Figure 8) (Halbach, Kriete, et al., 1989; Halbach, Sattler, et al., 1989; Koschinsky et al., 1997). Major phosphatization events throughout the geological history of FeMn crust formation in the Atlantic Ocean have been reported in previous studies (Benites et al., 2020, 2022; González et al., 2016; Josso et al., 2021; Marino et al., 2018). In our study, most of the FeMn crusts show phosphatization at their basal layers and show no primary remanent magnetization because these layers have undergone extensive diagenetic alteration (Figure 7 and Figure S1 in Supporting Information S1). Phosphate-rich suboxic water increases the replacement and recrystallization of unstable minerals through fractures and pores (Benites et al., 2020; Koschinsky et al., 1997).

In the phosphatized layers of the crust samples from RGR, acicular goethite (Figure S2 in Supporting Information S1) is the ordered phase of dehydration and recrystallization of pre-existing ferrihydrite, mediated by Fe-oxidizing bacteria (Benites et al., 2022). Goethite is also found in some hydrogenetic (non-phosphatized) and

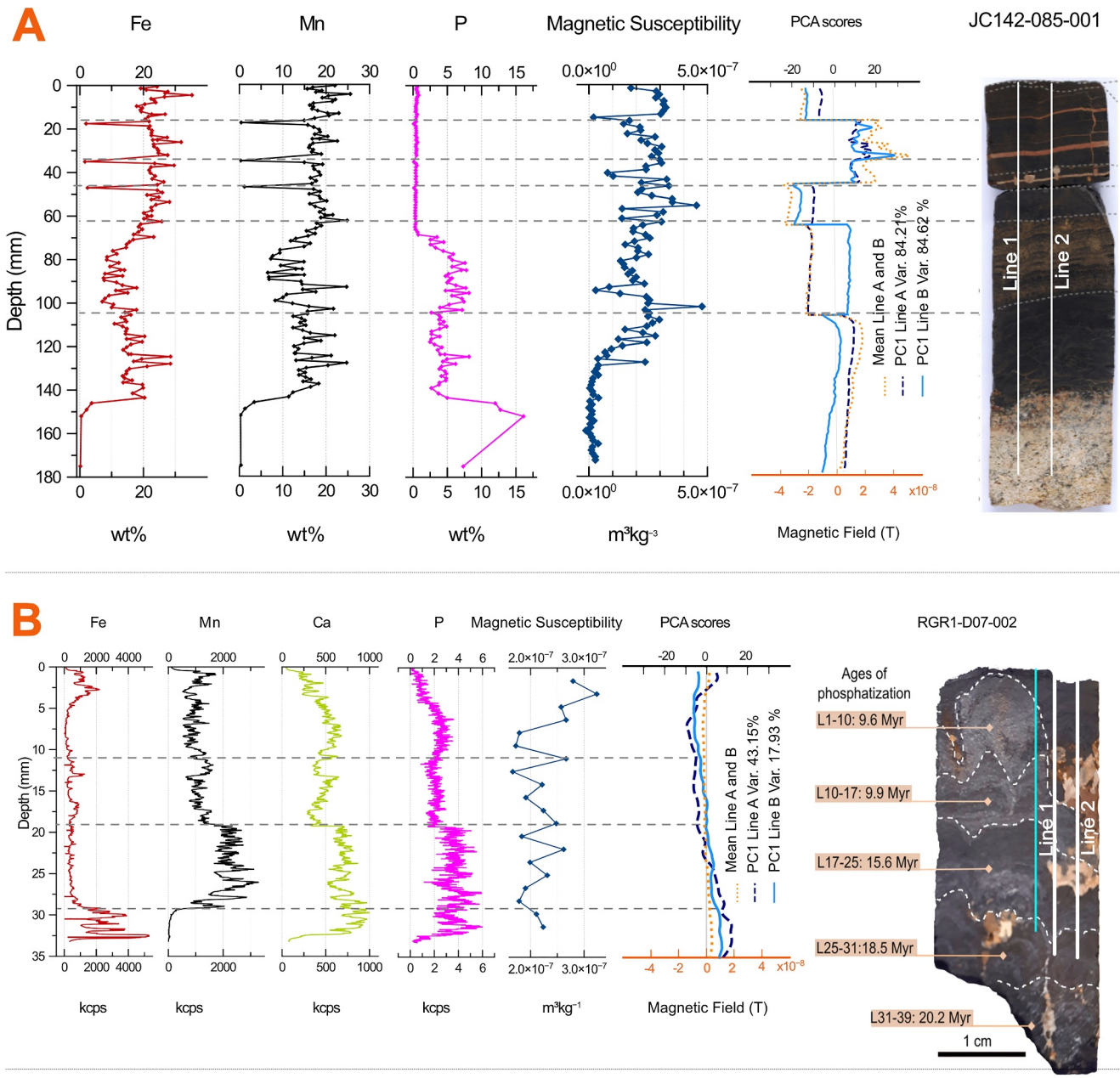

Figure 12. Geochemical versus Magnetic data along the crust samples from Rio Grande Rise (RGR) and TS: (a) Sample JC142-085-001 from Tropic Seamount, The continuous data for Fe, Mn and P was taken from Josso et al. (2019), where the sample was dated using $^{188}Os/^{187}Os$; the magnetic susceptibility was measured in discrete thin slice samples, Principal Component Analysis (PCA) score was obtained from the Hall probe magnetic scanning for two lines, Line A and B, and the mean of both lines is also shown in yellow dotted line; (b) Sample RGR1-D07-002 from RGR, The continuous data for Fe, Mn, Ca and P was taken from Benites et al. (2020) where the sample was dated using U-Th for non-phosphatized and $^{87}Sr/^{86}Sr$ for phosphatized crusts; the magnetic susceptibility was measured in discrete thin slice samples, PCA score was obtained from the Hall probe magnetic scanning for two lines, Line A and B, and the mean of both lines is also shown in yellow dotted line.

phosphatized layers of crust samples from TS. However, it is only present in some intervals along the crusts which are related to the dust input from the African continent and do not play a significant role in the primary remanent magnetization of FeMn crusts (Josso et al., 2019). Our magnetic, mineralogical and TEM data confirmed the presence of acicular goethite both in the RGR and on the TS. Goethite is a magnetic mineral with the potential of preserving primary remanent magnetization, however, most crystalline acicular goethite in FeMn crusts (i.e., the ordered and recrystallized form of pre-existing poorly crystalline Fe oxyhydroxides) is the result of diagenesis. Our results from the demagnetization (Figure S3 in Supporting Information S1) of sliced samples do not suggest

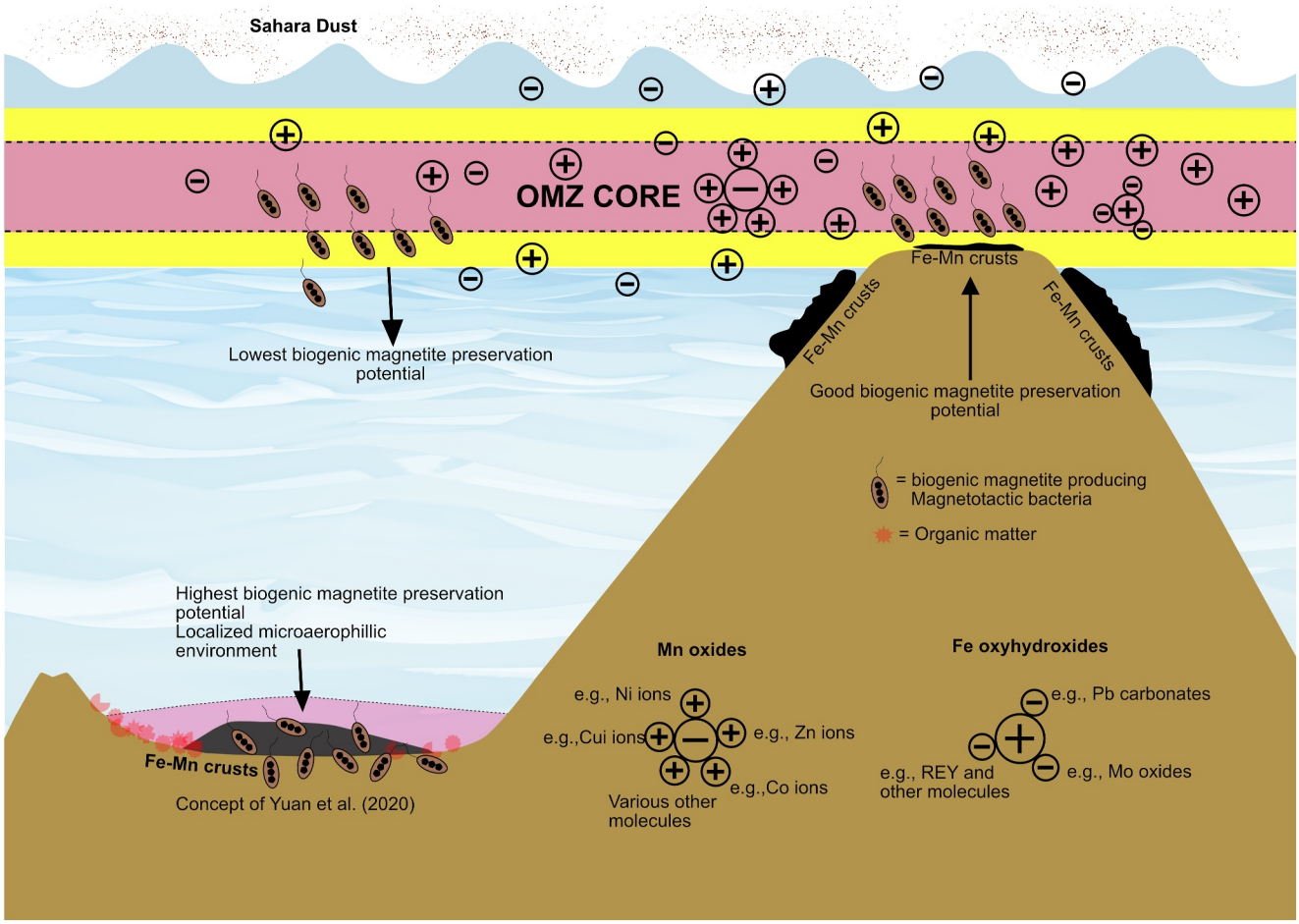

Figure 13. Schematic diagram for the possible preservation of biogenic magnetite produced by magnetotactic bacteria as a primary magnetic carrier in non-phosphatized FeMn crusts: Modified from Marino et al. (2017), the diagram incorporates the concept of Yuan et al. (2020) about the localized microaerophilic environment due to the corrosion of remains of planktons (organic matter). The concept of highest, good, and lowest biogenic magnetite preservation is from Larrasoaña et al. (2014).

the existence of primary magnetization recorded by goethite. Magnetic scanning data for the phosphatized layers of sample JC142-085-001 (TS) shows that the magnetic changes along the growth of the crust are driven by changes in Fe, Mn, P and Ca contents. Moreover, magnetic scanning data show a consistent magnetic change in erosive surfaces of FeMn crusts (Josso et al., 2019). These magnetic anomalies are not consistent with the expected magnetic response showing primary remanent magnetization. However, the magnetic response is related to the textural and geochemical changes along the crust. Since the phosphatized FeMn crusts are altered FeMn crusts, the magnetic minerals found in phosphatized layers would not reflect the original remanent magnetization.

6. Conclusions

We used geochemical, magnetic, mineralogical, and microscopic methods to understand the magnetic properties of FeMn crusts from RGR and TS. FeMn crusts from RGR and TS typically grow hydrogenetically under oxic conditions, preventing crystallization of primary remanent magnetization carrying magnetic minerals, and potentially causing oxidation of pre-existing magnetic minerals. The non-phosphatized layers in samples from both regions contain paramagnetic/superparamagnetic amorphous Fe oxyhydroxides which are not reliable for carrying primary remanent magnetization. Different phosphatization stages throughout the formation history of FeMn crusts have altered not only the primary geochemical and mineralogical signals but also the magnetic signals. CFA replace Fe and Mn-phases, promoting magnetic dilution. Moreover, during phosphatization magnetic minerals undergo sub-oxic dissolution, thereby losing their primary magnetic signals. Variations in magnetic parameters do not correspond to primary magnetization but rather to geochemical alterations. Extending the

interpretation of our results to the presence of magnetic minerals as primary remanent magnetization carriers in the Pacific Ocean and China Sea suggest that local environmental condition may be crucial for the preservation of these minerals, while the absence of Fe(II) is a common feature in FeMn crusts worldwide.

Data Availability Statement

Samples collection data are available from Jovane et al., 2019. Sample data collected during the cruise NBP1808 are available at https://earthref.org/ERESE/projects/NBP1808/. Sample data collected during the cruise DY094 are available at https://www.bodc.ac.uk/resources/inventories/cruise_inventory/search/. The data used in the study for the comparison are available from Josso et al. (2019) and Benites et al. (2020). Other data from this research are available at Hassan (2024a, 2024b).

Acknowledgments
We thank Prof. Luiz Carlos Nagamine from the Instituto de Física, Universidade de São Paulo for Mössbauer spectroscopy measurements and Prof. Fernanda Abreu from Instituto de Microbiologia Paulo de Góes, Universidade Federal do Rio de Janeiro for Transmission Electron Microscopy. We thank Mgr. Lucie Smrcinova for her help with multiple measurements utilizing the magnetic scanner at Charles University in Prague. We're grateful to the two anonymous reviewers for their thorough review and very constructive suggestions. MBH acknowledges PhD funding from FAPESP under project numbers 2017/04821-0 and 2021/06941-8. LJ acknowledges FAPESP support under project number 2016/24946-9. This study was also supported by the Project "Estudo Multidisciplinar de Novos Minerais Estratégicos e Avaliação de Risco da Mineração na Elevação de Rio Grande (Atlântico Sul) (e-MERG)," Ref. Finep nº 0013/21. G.K. was partially supported by the Czech Science Foundation, 23-06075S.

References

Ayers, J. M., & Strutton, P. G. (2013). Nutrient variability in subantarctic mode waters forced by the southern annular mode and ENSO. *Geophysical Research Letters*, *40*(13), 3419–3423. https://doi.org/10.1002/grl.50638

Barker, P. F., Johnson, R., Carlson, R. L., Johnson, D., Cepek, P., Coulbourn, W., et al. (1983). Site-516-Rio-Grande Rise. *Initial Reports of the Deep Sea Drilling Project*, *7*, 155–338. https://doi.org/10.2973/dsdp.proc.72.105.1983

Bau, M., & Koschinsky, A. (2006). Hafnium and neodymium isotopes in seawater and in ferromanganese crusts: The "element perspective". *Earth and Planetary Science Letters*, *241*(3–4), 952–961. https://doi.org/10.1016/j.epsl.2005.09.067

Bau, M. S. K. K., Schmidt, K., Koschinsky, A., Hein, J., Kuhn, T., & Usui, A. (2014). Discriminating between different genetic types of marine ferro-manganese crusts and nodules based on rare earth elements and yttrium. *Chemical Geology*, *381*, 1–9. https://doi.org/10.1016/j.chemgeo.2014.05.004

Bazylinski, D. A., & Frankel, R. B. (2004). Magnetosome formation in prokaryotes. *Nature Reviews Microbiology*, *2*(3), 217–230. https://doi.org/10.1038/nrmicro842

Benites, M., Hein, J. R., Mizell, K., Blackburn, T., & Jovane, L. (2020). Genesis and evolution of ferromanganese crusts from the summit of Rio Grande Rise, Southwest Atlantic Ocean. *Minerals*, *10*(4), 349. https://doi.org/10.3390/min10040349

Benites, M., Hein, J. R., Mizell, K., Farley, K. A., Treffkorn, J., & Jovane, L. (2022). Geochemical insights into formation of enigmatic ironstones from Rio Grande rise, South Atlantic Ocean. *Marine Geology*, *444*, 106716. https://doi.org/10.1016/j.margeo.2021.106716

Berndt, T. A., & Chang, L. (2019). Waiting for Forcot: Accelerating FORC processing 100× using a fast-Fourier-transform algorithm. *Geochemistry, Geophysics, Geosystems*, *20*(12), 6223–6233. https://doi.org/10.1029/2019gc008380

Bogdanova, O. Y., Gorshkov, A. I., Novikov, G. V., & Bogdanov, Y. A. (2008). Mineralogy of morphogenetic types of ferromanganese deposits in the world ocean. *Geology of Ore Deposits*, *50*(6), 462–469. https://doi.org/10.1134/s1075701508060044

Bonatti, E., Kraemer, T., & Rydell, H. (1972). Classification and genesis of submarine iron-manganese deposits. In D. R. Horn (Ed.), *Ferro-manganese deposits on the ocean floor* (pp. 149–166).

Brandt, P., Greatbatch, R. J., Claus, M., Didwischus, S. H., Hormann, V., Funk, A., et al. (2012). Ventilation of the equatorial Atlantic by the equatorial deep jets. *Journal of Geophysical Research*, *117*(C12), C12015. https://doi.org/10.1029/2012jc008118

Brandt, P., Hormann, V., Körtzinger, A., Visbeck, M., Krahmann, G., Stramma, L., et al. (2010). Changes in the ventilation of the oxygen minimum zone of the tropical North Atlantic. *Journal of Physical Oceanography*, *40*(8), 1784–1801. https://doi.org/10.1175/2010jpo4301.1

Camboa, L. A. P., & Rabinowitz, P. D. (1984). The evolution of the Rio Grande Rise in the southwest Atlantic Ocean. *Marine Geology*, *58*(1–2), 35–58. https://doi.org/10.1016/0025-3227(84)90115-4

Carpenter, R., & Wakeham, S. (1973). Mössbauer studies of marine and fresh water manganese nodules. *Chemical Geology*, *11*(2), 109–116. https://doi.org/10.1016/0009-2541(73)90047-8

Davidson, P., Koppers, A., Class, C., & Sager, W. (2022). A comprehensive geochronology study of the Rio Grande Rise: Evidence for prolonged on and off-ridge volcanism. *Authorea Preprints*.

Dymond, J., Lyle, M., Finney, B., Piper, D. Z., Murphy, K., Conard, R., & Pisias, N. (1984). Ferromanganese nodules from MANOP sites H, S, and R—Control of mineralogical and chemical composition by multiple accretionary processes. *Geochimica et Cosmochimica Acta*, *48*(5), 931–949. https://doi.org/10.1016/0016-7037(84)90186-8

Emerson, D., Roden, E., & Twining, B. (2012). The microbial ferrous wheel: Iron cycling in terrestrial, freshwater, and marine environments. *Frontiers in Microbiology*, *3*, 383. https://doi.org/10.3389/fmicb.2012.00383

Faivre, D., & Schuler, D. (2008). Magnetotactic bacteria and magnetosomes. *Chemical Reviews*, *108*(11), 4875–4898. https://doi.org/10.1021/cr078258w

Frank, M., O'nions, R. K., Hein, J. R., & Banakar, V. K. (1999). 60 Myr records of major elements and Pb–Nd isotopes from hydrogenous ferromanganese crusts: Reconstruction of seawater paleochemistry. *Geochimica et Cosmochimica Acta*, *63*(11–12), 1689–1708. https://doi.org/10.1016/s0016-7037(99)00079-4

Ganwani, G., Bhatia, B., Jaisankar, S., Pattan, J. N., Dixit, A., & Tripathi, R. P. (2017). MÖssbauer spectroscopy and X-ray diffraction studies of ferromanganese nodules from central Indian Ocean basin. *Journal of Applied Geochemistry*, *19*(3), 270–276.

González, F. J., Somoza, L., Hein, J. R., Medialdea, T., León, R., Urgorri, V., et al. (2016). Phosphorites, Co-rich Mn nodules, and Fe-Mn crusts from Galicia Bank, NE Atlantic: Reflections of Cenozoic tectonics and paleoceanography. *Geochemistry, Geophysics, Geosystems*, *17*(2), 346–374. https://doi.org/10.1002/2015gc005861

Guan, Y., Sun, X., Jiang, X., Sa, R., Zhou, L., Huang, Y., et al. (2017). The effect of Fe-Mn minerals and seawater interface and enrichment mechanism of ore-forming elements of polymetallic crusts and nodules from the South China Sea. *Acta Oceanologica Sinica*, *36*(6), 34–46. https://doi.org/10.1007/s13131-017-1004-4

Halbach, P., Kriete, C., Prause, B., & Puteanus, D. (1989). Mechanisms to explain the platinum concentration in ferromanganese seamount crusts. *Chemical Geology*, *76*(1–2), 95–106. https://doi.org/10.1016/0009-2541(89)90130-7

Halbach, P., & Puteanus, D. (1984). The influence of the carbonate dissolution rate on the growth and composition of Co-rich ferromanganese crusts from Central Pacific seamount areas. *Earth and Planetary Science Letters*, *68*(1), 73–87. https://doi.org/10.1016/0012-821x(84)90141-9

Halbach, P., Sattler, C. D., Teichmann, F., & Wahsner, M. (1989). Cobalt-rich and platinum-bearing manganese crust deposits on seamounts: Nature, formation, and metal potential. *Marine Mining*, *8*(1), 23–39.
Hassan, M. B. (2024a). Geochemical data of selected ferromanganese crust samples from Rio Grande Rise and Tropic Seamount. *Mendeley Data, V1*. https://doi.org/10.17632/33jctcjkd9.1
Hassan, M. B. (2024b). Supplementary file figures. *Mendeley Data, V1*. https://doi.org/10.17632/hn2dkjvwy4.1
Hassan, M. B., Rodelli, D., Benites, M., Abreu, F., Murton, B., & Jovane, L. (2020). Presence of biogenic magnetite in ferromanganese nodules. *Environmental Microbiology Reports*, *12*(3), 288–295. https://doi.org/10.1111/1758-2229.12831
Hein, J. R., Conrad, T. A., Frank, M., Christl, M., & Sager, W. W. (2012). Copper-nickel-rich, amalgamated ferromanganese crust-nodule deposits from Shatsky Rise, NW Pacific. *Geochemistry, Geophysics, Geosystems*, *13*(10), Q10022. https://doi.org/10.1029/2012gc004286
Hein, J. R., Conrad, T. A., & Staudigel, H. (2010). Seamount mineral deposits: A source of rare metals for high-technology industries. *Oceanography*, *23*(1), 184–189. https://doi.org/10.5670/oceanog.2010.70
Hein, J. R., & Koschinsky, A. (2014). Deep-ocean ferromanganese crusts and nodules.
Hein, J. R., Koschinsky, A., Bau, M., Manheim, F. T., Kang, J. K., & Roberts, L. (2000). *Cobalt-rich ferromanganese crusts in the Pacific*, *Handbook of marine mineral deposits* (Vol. 18, pp. 239–273). Routledge.
Hein, J. R., Koschinsky, A., & Halliday, A. N. (2003). Global occurrence of tellurium-rich ferromanganese crusts and a model for the enrichment of tellurium. *Geochimica et Cosmochimica Acta*, *67*(6), 1117–1127. https://doi.org/10.1016/s0016-7037(02)01279-6
Hein, J. R., Mizell, K., Koschinsky, A., & Conrad, T. A. (2013). Deep-ocean mineral deposits as a source of critical metals for high-and green-technology applications: Comparison with land-based resources. *Ore Geology Reviews*, *51*, 1–14. https://doi.org/10.1016/j.oregeorev.2012.12.001
Jiang, X., Zhao, X., Zhao, X., Chou, Y. M., Hein, J. R., Sun, X., et al. (2021). A magnetic approach to unravelling the paleoenvironmental significance of nanometer-sized Fe hydroxide in NW Pacific ferromanganese deposits. *Earth and Planetary Science Letters*, *565*, 116945. https://doi.org/10.1016/j.epsl.2021.116945
Jiang, X. D., Sun, X. M., Chou, Y. M., Hein, J. R., He, G. W., Fu, Y., et al. (2020). Geochemistry and origins of carbonate fluorapatite in seamount Fe–Mn crusts from the Pacific Ocean. *Marine Geology*, *423*, 106135. https://doi.org/10.1016/j.margeo.2020.106135
Jiang, X. D., Sun, X. M., & Guan, Y. (2019). Biogenic mineralization in the ferromanganese nodules and crusts from the South China Sea. *Journal of Asian Earth Sciences*, *171*, 46–59. https://doi.org/10.1016/j.jseaes.2017.07.050
Jiang, X. D., Zhao, X., Chou, Y. M., Liu, Q. S., Roberts, A. P., Ren, J. B., et al. (2020). Characterization and quantification of magnetofossils within abyssal manganese nodules from the Western Pacific Ocean and implications for nodule formation. *Geochemistry, Geophysics, Geosystems*, *21*(3), e2019GC008811. https://doi.org/10.1029/2019gc008811
Joshima, M., & Usui, A. (1998). Magnetostratigraphy of hydrogenetic manganese crusts from Northwestern Pacific seamounts. *Marine Geology*, *146*(1–4), 53–62. https://doi.org/10.1016/s0025-3227(97)00131-x
Josso, P., Lusty, P., Chenery, S., & Murton, B. (2021). Controls on metal enrichment in ferromanganese crusts: Temporal changes in oceanic metal flux or phosphatisation? *Geochimica et Cosmochimica Acta*, *308*, 60–74. https://doi.org/10.7185/gold2021.6110
Josso, P., Parkinson, I., Horstwood, M., Lusty, P., Chenery, S., & Murton, B. (2019). Improving confidence in ferromanganese crust age models: A composite geochemical approach. *Chemical Geology*, *513*, 108–119. https://doi.org/10.1016/j.chemgeo.2019.03.003
Jovane, L., Hein, J. R., Yeo, I. A., Benites, M., Bergo, N. M., Correa, P. V., et al. (2019). Multidisciplinary scientific cruise to the Rio Grande Rise. *Frontiers in Marine Science*, *6*, 252. https://doi.org/10.3389/fmars.2019.00252
Karlin, R. (1990). Magnetic mineral diagenesis in suboxic sediments at Bettis site W-N, NE Pacific Ocean. *Journal of Geophysical Research*, *95*(B4), 4421–4436. https://doi.org/10.1029/jb095ib04p04421
Kirschvink, J. (1980). The least-squares line and plane and the analysis of palaeomagnetic data. *Geophysical Journal International*, *62*(3), 699–718. https://doi.org/10.1111/j.1365-246x.1980.tb02601.x
Kletetschka, G., Schnabl, P., Šifnerová, K., Tasáryová, Z., Manda, Š., & Pruner, P. (2013). Magnetic scanning and interpretation of paleomagnetic data from Prague Synform's volcanics. *Studia Geophysica et Geodaetica*, *57*(1), 103–117. https://doi.org/10.1007/s11200-012-0723-4
Konstantinova, N., Cherkashov, G., Hein, J. R., Mirão, J., Dias, L., Madureira, P., et al. (2017). Composition and characteristics of the ferromanganese crusts from the western Arctic Ocean. *Ore Geology Reviews*, *87*, 88–99. https://doi.org/10.1016/j.oregeorev.2016.09.011
Kopp, R. E., & Kirschvink, J. L. (2008). The identification and biogeochemical interpretation of fossil magnetotactic bacteria. *Earth-Science Reviews*, *86*(1–4), 42–61. https://doi.org/10.1016/j.earscirev.2007.08.001
Koschinsky, A., Halbach, P., Hein, J. R., & Mangini, A. (1996). Ferromanganese crusts as indicators for paleoceanographic events in the NE Atlantic. *Geologische Rundschau*, *85*(3), 567–576. https://doi.org/10.1007/bf02369011
Koschinsky, A., & Hein, J. R. (2003). Uptake of elements from seawater by ferromanganese crusts: Solid-phase associations and seawater speciation. *Marine Geology*, *198*(3–4), 331–351. https://doi.org/10.1016/s0025-3227(03)00122-1
Koschinsky, A., & Hein, J. R. (2017). Marine ferromanganese encrustations: Archives of changing oceans. *Elements: An International Magazine of Mineralogy, Geochemistry, and Petrology*, *13*(3), 177–182. https://doi.org/10.2113/gselements.13.3.177
Koschinsky, A., Stascheit, A., Bau, M., & Halbach, P. (1997). Effects of phosphatization on the geochemical and mineralogical composition of marine ferromanganese crusts. *Geochimica et Cosmochimica Acta*, *61*(19), 4079–4094. https://doi.org/10.1016/s0016-7037(97)00231-7
Koschinsky, A., Van Gerven, M., & Halbach, P. (1995). First investigations of massive ferromanganese crusts in the NE Atlantic in comparison with hydrogenetic Pacific occurrences. *Marine Georesources & Geotechnology*, *13*(4), 375–391. https://doi.org/10.1080/10641199509388294
Kuhn, T., Bau, M., Blum, N., & Halbach, P. (1998). Origin of negative Ce anomalies in mixed hydrothermal–hydrogenetic Fe–Mn crusts from the Central Indian Ridge. *Earth and Planetary Science Letters*, *163*(1–4), 207–220. https://doi.org/10.1016/s0012-821x(98)00188-5
Larrasoaña, J. C., Liu, Q., Hu, P., Roberts, A. P., Mata, P., Civis, J., et al. (2014). Paleomagnetic and paleoenvironmental implications of magnetofossil occurrences in late Miocene marine sediments from the Guadalquivir Basin, SW Spain. *Frontiers in Microbiology*, *5*, 71. https://doi.org/10.3389/fmicb.2014.00071
Liu, Q., Roberts, A. P., Larrasoana, J. C., Banerjee, S. K., Guyodo, Y., Tauxe, L., & Oldfield, F. (2012). Environmental magnetism: Principles and applications. *Reviews of Geophysics*, *50*(4), RG4002. https://doi.org/10.1029/2012rg000393
Lurcock, P. C., & Wilson, G. S. (2012). PuffinPlot: A versatile, user-friendly program for paleomagnetic analysis. *Geochemistry, Geophysics, Geosystems*, *13*(6), Q06Z45. https://doi.org/10.1029/2012gc004098
Manheim, F. T., & Lane-Bostwick, C. M. (1988). Cobalt in ferromanganese crusts as a monitor of hydrothermal discharge on the Pacific sea floor. *Nature*, *335*(6185), 59–62. https://doi.org/10.1038/335059a0
Marino, E., González, F. J., Kuhn, T., Madureira, P., Wegorzewski, A. V., Mirao, J., et al. (2019). Hydrogenetic, diagenetic and hydrothermal processes forming ferromanganese crusts in the Canary Island Seamounts and their influence in the metal recovery rate with hydrometallurgical methods. *Minerals*, *9*(7), 439. https://doi.org/10.3390/min9070439

Marino, E., González, F. J., Lunar, R., Reyes, J., Medialdea, T., Castillo-Carrión, M., et al. (2018). High-resolution analysis of critical minerals and elements in Fe–Mn crusts from the Canary Island Seamount Province (Atlantic Ocean). *Minerals*, *8*(7), 285. https://doi.org/10.3390/min8070285

Marino, E., González, F. J., Somoza, L., Lunar, R., Ortega, L., Vázquez, J. T., et al. (2017). Strategic and rare elements in Cretaceous-Cenozoic cobalt-rich ferromanganese crusts from seamounts in the Canary Island Seamount Province (northeastern tropical Atlantic). *Ore Geology Reviews*, *87*, 41–61. https://doi.org/10.1016/j.oregeorev.2016.10.005

Maxbauer, D. P., Feinberg, J. M., Fox, D. L., & Clyde, W. C. (2016). Magnetic minerals as recorders of weathering, diagenesis, and paleoclimate: A core–outcrop comparison of Paleocene–Eocene paleosols in the Bighorn Basin, WY, USA. *Earth and Planetary Science Letters*, *452*, 15–26. https://doi.org/10.1016/j.epsl.2016.07.029

Murad, E., & Schwertmann, U. (1988). Iron oxide mineralogy of some deep-sea ferromanganese crusts. *American Mineralogist*, *73*(11–12), 1395–1400.

Noguchi, A., Oda, H., Yamamoto, Y., Usui, A., Sato, M., & Kawai, J. (2017). Scanning SQUID microscopy of a ferromanganese crust from the northwestern Pacific: Submillimeter scale magnetostratigraphy as a new tool for age determination and mapping of environmental magnetic parameters. *Geophysical Research Letters*, *44*(11), 5360–5367. https://doi.org/10.1002/2017gl073201

Noguchi, A., Yamamoto, Y., Nishi, K., Usui, A., & Oda, H. (2017). Paleomagnetic study of ferromanganese crusts recovered from the northwest Pacific—Testing the applicability of the magnetostratigraphic method to estimate growth rate. *Ore Geology Reviews*, *87*, 16–24. https://doi.org/10.1016/j.oregeorev.2016.07.018

Oda, H., Katanoda, W., Usui, A., Murayama, M., & Yamamoto, Y. (2023). Rotation of a ferromanganese nodule in the Penrhyn Basin, South Pacific, tracked by the Earth's magnetic field. *Geochemistry, Geophysics, Geosystems*, *24*(3), e2022GC010789. https://doi.org/10.1029/2022gc010789

Oda, H., Nakasato, Y., & Usui, A. (2018). Characterization of marine ferromanganese crust from the Pacific using residues of selective chemical leaching: Identification of fossil magnetotactic bacteria with FE-SEM and rock magnetic methods. *Earth Planets and Space*, *70*(1), 1–10. https://doi.org/10.1186/s40623-018-0924-3

Oda, H., Usui, A., Miyagi, I., Joshima, M., Weiss, B. P., Shantz, C., et al. (2011). Ultrafine-scale magnetostratigraphy of marine ferromanganese crust. *Geology*, *39*(3), 227–230. https://doi.org/10.1130/g31610.1

Palomino, D., Vázquez, J. T., Somoza, L., León, R., López-González, N., Medialdea, T., et al. (2016). Geomorphological features in the southern Canary Island Volcanic Province: The importance of volcanic processes and massive slope instabilities associated with seamounts. *Geomorphology*, *255*, 125–139. https://doi.org/10.1016/j.geomorph.2015.12.016

Pattan, J. N., & Mudholkar, A. V. (1991). Mössbauer studies and oxidized manganese ratio in ferromanganese nodules and crusts from the Central Indian Ocean. *Geo-Marine Letters*, *11*(1), 51–55. https://doi.org/10.1007/bf02431055

Roberts, A. P. (2015). Magnetic mineral diagenesis. *Earth-Science Reviews*, *151*, 1–47. https://doi.org/10.1016/j.earscirev.2015.09.010

Roberts, A. P., Florindo, F., Villa, G., Chang, L., Jovane, L., Bohaty, S. M., et al. (2011). Magnetotactic bacterial abundance in pelagic marine environments is limited by organic carbon flux and availability of dissolved iron. *Earth and Planetary Science Letters*, *310*(3–4), 441–452. https://doi.org/10.1016/j.epsl.2011.08.011

Rodelli, D., Jovane, L., Giorgioni, M., Rego, E. S., Cornaggia, F., Benites, M., et al. (2019). Diagenetic fate of biogenic soft and hard magnetite in chemically stratified sedimentary environments of Mamanguá Ría, Brazil. *Journal of Geophysical Research: Solid Earth*, *124*(3), 2313–2330. https://doi.org/10.1029/2018jb016576

Rodelli, D., Jovane, L., Roberts, A. P., Cypriano, J., Abreu, F., & Lins, U. (2018). Fingerprints of partial oxidation of biogenic magnetite from cultivated and natural marine magnetotactic bacteria using synchrotron radiation. *Environmental Microbiology Reports*, *10*(3), 337–343. https://doi.org/10.1111/1758-2229.12644

Rusanov, V., Chakarova, K., & Trautwein, A. X. (2008). On the possibility to use stratabound hydrothermal crusts as indicators for local or global changes in the environment. *Journal of Atmospheric and Solar-Terrestrial Physics*, *70*(2–4), 285–292. https://doi.org/10.1016/j.jastp.2007.08.017

Sarmiento, J. L., Gruber, N., Brzezinski, M. A., & Dunne, J. P. (2004). High-latitude controls of thermocline nutrients and low latitude biological productivity. *Nature*, *427*(6969), 56–60. https://doi.org/10.1038/nature02127

Savelyev, D. P., Savelyeva, O. L., Moskaleva, S. V., & Rashidov, V. A. (2022). Composition of cosmic spherules from ferromanganese crusts of the Magellan Seamounts. *Geochemistry International*, *60*(5), 411–420. https://doi.org/10.1134/s0016702922050081

Sergipe, P. P., Louro, V., Marangoni, Y. R., de Moura, D. S., & Jovane, L. (2023). A study of volcanic rocks and ferromanganese crusts through marine geophysical methods integration in the north portion of Cruzeiro do Sul Rift in the Rio Grande Rise. *Frontiers in Marine Science*, *10*. https://doi.org/10.3389/fmars.2023.1093108

Sousa, I. M. C., Santos, R. V., Koschinsky, A., Bau, M., Wegorzewski, A. V., Cavalcanti, J. A. D., & Dantas, E. L. (2021). Mineralogy and chemical composition of ferromanganese crusts from the Cruzeiro do Sul Lineament-Rio Grande Rise, South Atlantic. *Journal of South American Earth Sciences*, *108*, 103207. https://doi.org/10.1016/j.jsames.2021.103207

Staszak, P., Collot, J., Josso, P., Pelleter, E., Etienne, S., Patriat, M., et al. (2022). Origin and composition of ferromanganese deposits of New Caledonia Exclusive Economic Zone. *Minerals*, *12*(2), 255. https://doi.org/10.3390/min12020255

Strehlau, J. H., Hegner, L. A., Strauss, B. E., Feinberg, J. M., & Penn, R. L. (2014). Simple and efficient separation of magnetic minerals from speleothems and other carbonates. *Journal of Sedimentary Research*, *84*(11), 1096–1106. https://doi.org/10.2110/jsr.2014.89

Stumm, W., Morgan, J. J., & Drever, J. I. (1996). Aquatic chemistry. *Journal of Environmental Quality*, *25*(5), 1162. https://doi.org/10.2134/jeq1996.00472425002500050033x

Templeton, A. S., Knowles, E. J., Eldridge, D. L., Arey, B. W., Dohnalkova, A. C., Webb, S. M., et al. (2009). A seafloor microbial biome hosted within incipient ferromanganese crusts. *Nature Geoscience*, *2*(12), 872–876. https://doi.org/10.1038/ngeo696

Terashima, S., Usui, A., & Imai, N. (1995). Two new GSJ geochemical reference samples: Syenite JSy-1 and manganese nodule JMn-1. *Geostandards Newsletter*, *19*(2), 221–229. https://doi.org/10.1111/j.1751-908x.1995.tb00160.x

Usui, A., Graham, I. J., Ditchburn, R. G., Zondervan, A., Shibasaki, H., & Hishida, H. (2007). Growth history and formation environments of ferromanganese deposits on the Philippine Sea Plate, northwest Pacific Ocean. *Island Arc*, *16*(3), 420–430. https://doi.org/10.1111/j.1440-1738.2007.00592.x

Usui, A., Nishi, K., Sato, H., Nakasato, Y., Thornton, B., Kashiwabara, T., et al. (2017). Continuous growth of hydrogenetic ferromanganese crusts since 17 Myr ago on Takuyo-Daigo Seamount, NW Pacific, at water depths of 800–5500 m. *Ore Geology Reviews*, *87*, 71–87. https://doi.org/10.1016/j.oregeorev.2016.09.032

Usui, A., & Someya, M. (1997). Distribution and composition of marine hydrogenetic and hydrothermal manganese deposits in the northwest Pacific. *Geological Society, London, Special Publications*, *119*(1), 177–198. https://doi.org/10.1144/gsl.sp.1997.119.01.12

Varentsov, I. M., Drits, V. A., Gorshkov, A. I., Sivtsov, A. T., & Sakharov, B. A. (1991). Mn-Fe oxyhydroxide crusts from Krylov Seamount (eastern Atlantic): Mineralogy, geochemistry and genesis. *Marine Geology*, *96*(1–2), 53–70. https://doi.org/10.1016/0025-3227(91)90201-e

Xu, X., Qiang, X., Zhao, H., & Fu, C. (2020). Magnetic mineral dissolution recorded in a lacustrine sequence from the Heqing Basin, SW China, and its relationship with changes in the Indian monsoon. *Journal of Asian Earth Sciences*, *188*, 104081. https://doi.org/10.1016/j.jseaes.2019.104081

Yamazaki, T. (2020). Reductive dissolution of biogenic magnetite. *Earth Planets and Space*, *72*(1), 1–9. https://doi.org/10.1186/s40623-020-01290-3

Yamazaki, T., & Ikehara, M. (2012). Origin of magnetic mineral concentration variation in the Southern Ocean. *Paleoceanography*, *27*(2), PA2206. https://doi.org/10.1029/2011pa002271

Yi, L., Medina-Elizalde, M., Kletetschka, G., Yao, H., Simon, Q., Paterson, G. A., et al. (2020). The potential of marine ferromanganese nodules from Eastern Pacific as recorders of Earth's magnetic field changes during the past 4.7 Myr: A geochronological study by magnetic scanning and authigenic $^{10}Be/^{9}Be$ dating. *Journal of Geophysical Research: Solid Earth*, *125*(7), e2019JB018639. https://doi.org/10.1029/2019jb018639

Yi, L., Medina-Elizalde, M., Tan, L., Kemp, D. B., Li, Y., Kletetschka, G., et al. (2023). Plio-Pleistocene deep-sea ventilation in the eastern Pacific and potential linkages with Northern Hemisphere glaciation. *Science Advances*, *9*(8), eadd1467. https://doi.org/10.1126/sciadv.add1467

Yuan, W., Zhou, H., Yang, Z., Hein, J. R., & Yang, Q. (2020). Magnetite magnetofossils record biogeochemical remanent magnetization in hydrogenetic ferromanganese crusts. *Geology*, *48*(3), 298–302. https://doi.org/10.1130/g46881.1

Yuan, W., Zhou, H., Zhao, X., Yang, Z., Yang, Q., & Zhu, B. (2017). Magnetic stratigraphic dating of marine hydrogenetic ferromanganese crusts. *Scientific Reports*, *7*(1), 16748. https://doi.org/10.1038/s41598-017-17077-8